chemengineering

MDPI

Article

Layered Double Hydroxide Sorbents for Removal of Selenium from Power Plant Wastewaters

Man Li [1,2], Tanzil Chowdhury [1,2], Andrea N. Kraetz [2,3], Hangkun Jing [1,2], Andrew Dopilka [1,2], Lisa M. Farmen [4], Shahnawaz Sinha [2,5] and Candace K. Chan [1,2,*]

1 Materials Science and Engineering, School for Engineering of Matter, Transport and Energy, Arizona State University, Tempe, AZ 85287, USA; riemann89@asu.edu (M.L.); tachowd1@asu.edu (T.C.); hjing4@asu.edu (H.J.); adopilka@asu.edu (A.D.)
2 Nanosystems Engineering Research Center for Nanotechnology-Enabled Water Treatment, Arizona State University, Tempe, AZ 85287, USA; akraetz@asu.edu (A.N.K.); Shahnawaz.Sinha@asu.edu (S.S.)
3 Chemical Engineering, School for Engineering of Matter, Transport and Energy, Arizona State University, Tempe, AZ 85287, USA
4 Crystal Clear Technologies, Inc., Portland, OR 97201, USA; Lisa@crystalcleartechnology.us
5 School of Sustainable Engineering and the Built Environment, Arizona State University, Tempe, AZ 85287, USA
* Correspondence: Candace.Chan@asu.edu; Tel.: +1-(480)-727-8614

Received: 28 December 2018; Accepted: 20 February 2019; Published: 22 February 2019

Abstract: Selenium is an essential trace element but is increasingly becoming a contaminant of concern in the electric power industry due to the challenges of removing solubilized selenate anions, particularly in the presence of sulfate. In this work, we evaluate granulated layered double hydroxide (LDH) materials as sorbents for selenium removal from wastewaters obtained from a natural gas power plant with the aim to elucidate the effect of competing ions on the sorption capacities for selenium removal. We first present jar test data, followed by small-scale column testing in 0.43 inch (1.1 cm) and 2 inch (5.08 cm) diameter testbed columns for the treatment of as-obtained cooling tower blowdown waters and plant wastewaters. Finally, we present field results from a pilot-scale study evaluating the LDH media for treatment of cooling tower blowdown water. We find that despite the high levels of total dissolved solids and competing sulfate ions, the selenium oxoanions and other regulated metals such as chromium and arsenic are successfully removed using LDH media without needing any pre-treatment or pH adjustment of the wastewater.

Keywords: Layered double hydroxide; selenium; sorbent; column test; cooling tower blowdown; industrial wastewater treatment

1. Introduction

Selenium removal from electric power plant wastewaters has received much attention recently due to the revised effluent limitations guidelines (ELG) for steam electric power plants published by the U.S. Environmental Protection Agency in 2015 [1]. The purpose of these ELGs was to set new, more stringent federal limits on the levels of pollutants that can be discharged in wastewaters from power plants, notably toxic and bioaccumulative pollutants such as arsenic, mercury, selenium, chromium, and cadmium. For example, under these guidelines, the maximum average daily concentration limit for selenium in flue gas desulfurization (FGD) wastewaters from existing sources is 12 μg/L over 30 consecutive days; for new sources the limit is 5 μg/L [1,2]. In cases where wastewater is discharged to surface waters used by aquatic wildlife, the discharge limit can be lower due to ecological and health risks [3] (e.g., 2 μg/L in the state of Arizona [4]). The high rates of deformity and mortality in birds and fish in the Kesterson National Wildlife Refuge in California in the 1980s from

agricultural drainage containing average selenium concentrations of 300 µg/L [5,6] is a stark example of the potential harmful effects of selenium in the aquatic environment.

The fundamental challenges and treatment technologies for selenium have been highlighted in several reviews [2,7–10] and include chemical, physical, and biological methods, with bioreactors containing selenium-reducing microorganisms being one of the most mature technologies that have been evaluated for pilot and full-scale wastewater treatment [11,12]. However, some of these bacteria are sensitive to other anions in the water (e.g., chloride, nitrate) [2], and waters containing high levels of sulfate may encourage growth of sulfate-reducing bacteria, which can compete with selenium-reducing bacteria for nutrients [12]. Moreover, biological treatment requires larger footprints with longer residence times (4–6 hours) compared to physicochemical processes to remove selenium [8]. For these reasons, alternative technologies such as sorption are receiving interest for further development [9]. Selenium is mostly found as the selenate oxoanion, SeO_4^{2-}, in aerobic environments, which is difficult to remove via adsorption due to its tendency to bind via outer sphere mechanisms on common sorbents [13–16]. This, along with its chemical and physical similarities to sulfate, make selectivity of common sorbents to selenate a challenge.

Layered double hydroxides (LDHs) [17] are attractive as sorbents and ion-exchange media for a wide number of anions and oxoanions [18], as well as certain cations [19] and radionuclides [20]. LDHs, also known as hydrotalcite-like compounds, can be represented as $[M^{II}_{1-x}M^{III}_x(OH)_2]^{x+}[A^{n-}_{x/n}]^{x-}\cdot mH_2O$, where M^{II} = divalent metals such as Mg^{2+}, Zn^{2+}, Co^{2+}, Cu^{2+}; M^{III} = trivalent metals such as Al^{3+}, Fe^{3+}, Ni^{3+}, etc., that form brucite-like layers; A^{n-} is an exchangeable anion with a valence of n; and the x value is in the range of $0.20 \leq x \leq 0.33$ [21,22]. The presence of trivalent metals in the structure makes LDHs positively charged with high point of zero charge (pH_{pzc} around 8–12.5 depending on the composition) [18], and interlayer anions can be exchanged to preserve charge balance. Numerous reports have shown that LDH-based materials are promising sorbents for removing both selenate, Se(VI), and selenite, Se(IV), oxoanions [23–43], but these were largely fundamental studies performed in batch (jar) tests. The removal mechanism for selenite (as $HSeO_3^-$) on LDH is proposed as a combination of ion-exchange with interlayer carbonate anions and some chemisorption, while selenate is removed by ion-exchange with interlayer carbonate and surface hydroxide ions [25,29,31].

There have been only a few studies looking at the evaluation of LDH sorbents for selenium removal under dynamic conditions in column tests [29,36,44]. We recently investigated the removal of selenium from natural ground water using granulated LDH ($M^{II} = Mg^{2+}$, $M^{III} = Al^{3+}$, $A = CO_3^{2-}$) in small-scale column tests [44]. We found that the LDH was effective for removing trace levels of selenium from ground water containing much higher concentrations of sulfate, e.g., [Se] < 2 ppb vs. [S] ~40 parts-per-million (ppm), a difference of more than 20,000. Although the LDH did not display good selectivity for selenium over sulfate, the high anion adsorption capacities still enabled the simultaneous removal of both types of oxoanions.

In this work, we evaluate the LDH sorption capacities for selenium in wastewaters obtained from a natural gas power plant that utilized the aforementioned ground water as make-up waters for the cooling water. In general, a large amount of water is required to extract heat from the power plant condenser on the low pressure side of the steam turbine and dissipate it in the wet cooling towers through evaporation [45]. The ions in the water can then become concentrated in the cooling tower blowdown during the evaporation. This not only could potentially cause issues for meeting discharge limits for restricted contaminants, but also could increase the salinity of the waters and affect treatment.

Therefore, the aim of this study was to assess the ability of the LDH media to remove selenium from more complex wastewater streams containing higher levels of sulfate. Further, as LDHs are known to remove many types of organic and inorganic contaminants, the concurrent removal of other species was investigated. The practical application of LDH granulated sorbents in dynamic sorption tests using small-scale (1.1 cm), testbed (2 inch = 5.08 cm), and pilot-scale (3 inch = 7.62 cm) columns was investigated for the treatment of power plant wastewaters and to evaluate the scaling ability of this treatment approach. A post-mortem analysis of the LDH materials after the column tests was

conducted to elucidate the removal mechanism of contaminants. Finally, the stability and recyclability of the LDH media were addressed.

2. Materials and Methods

2.1. Sorbent Materials

Granular mixed metal oxide (61.7% MgO, 38.3% Al_2O_3 by weight) media was obtained from Sasol Germany GmbH (PURALOX MG 63 HT–Granulate) for column tests. Prior to use, the granules were immersed in de-ionized water in order to rehydrate the media and form the layered double hydroxide (LDH) structure. The rehydrated media (from now on, referred to as "granular LDH"), was loaded into the column as a slurry in order to avoid heat generation upon initiation of water flow into the bed and prevent entrapment of air bubbles. Unless otherwise noted, jar tests were performed using a powdered surrogate material (from now on, referred to as "LDH-500C") due to the tendency of the granulated media to undergo attrition under vigorous shaking or magnetic stirring. A scheme summarizing the sorbent structure (as-obtained and after processing) for both granular and powdered forms can be found in Scheme S1.

2.2. Water Samples

Synthetic water samples used in jar tests were prepared from sodium selenite and selenate salts dissolved in de-ionized (DI) water. Wastewater samples were obtained from Salt River Project's Santan Generating Station, a combined cycle, natural-gas-powered plant in Gilbert, AZ. The boiler and cooling water for Santan Generation Station were sourced from ground water from onsite wells or from surface waters from canals containing naturally occurring levels of selenium. Samples from the make-up water (canal and well water), canal water after clarification and water treatment, cooling tower blowdown, and final plant discharge waste were chosen for this investigation. Inductively coupled plasma coupled with optical emission spectroscopy (ICP-OES) or mass spectrometry (ICP-MS) were used to quantify the Se and S in the water samples. More details regarding the preparation and analysis of water samples are in the Supplementary Materials.

2.3. Jar Testing

To assess the fundamental adsorption capacities for LDH removal of Se(VI), equilibrium adsorption isotherms were performed in jar tests containing DI water spiked with Na_2SeO_4 using the LDH-500C powder at a dosage of 1 g/L and contact time of 22 h. Experimental data were fit to the Langmuir model. Se(VI) removal from wastewater samples spiked with 0.2 ppm Se(VI) was studied using LDH-500C at dosages between 1–5 g/L with contact time of 22 h. The stability of the as-obtained granules was assessed by agitating the media in various solutions (e.g., DI water with and without Se(VI) and NaOH) and measuring the Mg^{2+} and Al^{3+} levels with ICP-MS. To investigate the regeneration of spent LDH media, LDH-500C (5 g/L) was saturated with selenate or sulfate through exposure to 50 ppm solutions prepared from Na_2SeO_4 or Na_2SO_4 dissolved in DI water. The saturated media was then regenerated by calcination at 550 °C for 2 h in a box oven in air. The regenerated LDH-500C was then exposed to subsequent cycles of Se(VI) adsorption (50 ppm, 3 h contact time) and regeneration. More details regarding the jar tests are in the Supplementary Materials.

2.4. Column Testing

The granular LDH was evaluated in a 1.1 cm diameter column using up-flow mode and an empty-bed contact time (EBCT) of 30 min for the treatment of cooling tower (CT) blowdown water. For the scaled-up evaluation of the media, a testbed comprising three identical columns 2" (5.08 cm) in diameter was used in a serial flow configuration (up-flow mode) for the treatment of the CT blowdown and power plant discharge waters. Each column test was run continuously to assess approximately 1000 bed volumes of operation. For pilot-scale testing, a skid consisting of 3" diameter (7.62 cm) and

60" (152.4 cm) high columns was used for online treatment of CT blowdown at the Salt River Project Santan Generating Station. The pilot test was limited to ~100 gal of water. More details regarding the column test conditions are in the Supplementary Materials.

3. Results

3.1. Physical Properties of LDH

The physical properties of the granular LDH used in the column tests of this study were already investigated in our prior work [44,46], which established that the as-obtained, mixed metal oxide material exhibited the cubic periclase structure of a magnesium/aluminum solid solution, which is typically obtained when LDH is calcined at high temperatures to remove interlayer water and anions [47–49]. Upon re-introduction of the granules to DI water, the layered double hydroxide structure was successfully recovered [44] in what is known as the "memory effect" of LDHs [38]. This memory effect can also be exploited to remove anions from water, as they are captured by the LDH when the layered structure is reconstructed. However, in our case, the granules were rehydrated in DI water prior to use in the column tests. Hence, the granular media exhibited the layered structure during use and removal of ions would proceed via surface adsorption and anion-exchange with carbonate and hydroxide species, without the extra removal capacity arising from the memory effect.

XRD and FTIR characterization showed that the as-obtained LDH powder had a layered structure but the powder was too hydrophobic to disperse into water for the jar tests. After calcination at 500 °C, the powder (referred to as LDH-500C) could be easily dispersed into water and displayed the mixed metal oxide structure (Figures S1 and S2). Hence, LDH-500C could be used to capture anions using the memory effect discussed above, in addition to surface adsorption and anion-exchange [44]. The reconstruction of the layered structure via the memory effect once LDH-500C was exposed to water solutions containing selenate was also confirmed (Figure S1). Despite the difference in structure for the granular LDH (i.e., layered) and LDH-500C powder (i.e., non-layered) (Scheme S1), the latter was used as a surrogate for most of the jar tests described in Section 2.3 due to the ease of precisely measuring the dosage of dry sorbents.

3.2. Jar Testing of LDH

The equilibrium adsorption isotherms showed a good fit to the Langmuir model (Figure 1, Supplementary Materials); the calculated maximum capacity (Q_{max}) and the equilibrium constant were 66 ± 0.65 mg/g and 0.14 L/mg, respectively. Given that LDH-500C was calcined, the actual adsorption capacity of the non-calcined layered media used in the column tests was likely around 30 mg/g, on the basis of previous reports showing selenium sorption on non-calcined LDH to be about half that of the calcined form [38,44] and assuming no decrease in adsorption capacity due to granulation (justified on account of the similar surface area, i.e., 188 m^2/g for the granules vs. 179 m^2/g for the calcined powder). Due to differences in sorbent dosages and pH conditions used in isotherm experiments, it is not straightforward to compare the Q_{max} values obtained here to others from the literature. Nonetheless, reported Se(VI) adsorption capacities for sorbents based on aluminum oxides [50], iron oxides [51–53], manganese oxides [54,55], chitosan/clay [56], and silica [57] have all been below 20 mg/g. A study on crystalline Mg-Al LDHs prepared using different synthetic methods reported adsorption capacities as high as 45 mg/g [27], which is consistent with our findings here that LDH media can display superior adsorption capacities for Se(VI) compared to other metal oxide sorbents.

The sorption kinetics of the granular LDH were already studied and reported in our previous study [46] and displayed a good fit to a pseudo-second order model, with equilibrium reached within 4 h for removal of both Se(VI) and Se(IV) oxoanions from DI water solutions. Hence, these results demonstrate the large adsorption ability and fast kinetics of the LDH materials for removing selenium in deionized water solutions free from competing ions.

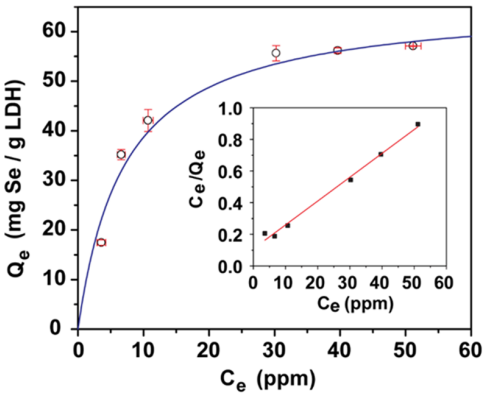

Figure 1. Adsorption isotherms of 1 g/L LDH-500C in spiked de-ionized (DI) water solutions containing Se(VI) using 22 h exposure time; inset shows the Langmuir plot.

LDH-500C was further studied for removal of selenate from various power plant wastewaters, which are schematically shown in Figure 2a. The pH values of the wastewaters were measured immediately after the sampling and ranged from 6.88 to 8.42, as shown in Table S1. Due to the low, parts-per-billion (ppb) natural levels of selenium in the as-obtained water samples (see Table S1), 0.2 ppm Se(VI) was spiked into the wastewaters. Figure 2b shows the amount of Se(VI) removed after 0.5 min, 2 h, and 22 h when using LDH-500C dosages of 1 g/L and 5 g/L.

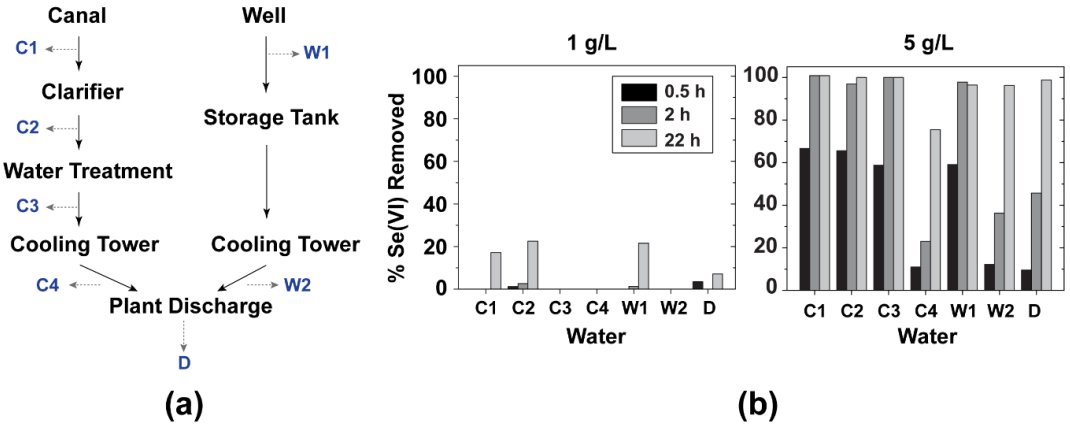

Figure 2. (**a**) Schematic showing the water sampling sites at the power plant; (**b**) Jar test results from power plant waters spiked with 0.2 ppm selenate using LDH-500C at 1 g/L and 5 g/L dosage.

The results showed that although LDH-500C displayed good Se(VI) sorption capacities and kinetics in the spiked DI water samples, the performance was worse in the various wastewater samples. Using a dosage of 1 g/L, no more than 30% of the Se(VI) could be removed from the spiked wastewaters, with the highest efficacy observed when LDH-500C was used to treat the upstream waters (e.g., raw and clarified canal water, raw well water). The differences in removal efficacy presumably originated from the different levels of background ions in the different waters, as the ions become concentrated in the cooling tower blowdown. From historical data obtained from the power plant [58], the sulfate concentrations in the cooling tower blowdown range from 500–700 ppm, while the sulfate concentrations in the ground and surface waters that supply the make-up water are typically below 100 ppm. Due to the similar chemical and physical properties of sulfate and selenate, the two oxoanions can compete with the same sites on the LDH [59], which means that higher dosages of sorbent are required to fully remove the Se(VI).

Using the well water (W1) as an example, the LDH-500C dosage was increased from 1 to 5 g/L and the Se(VI) removal efficacy after 22 h exposure was compared (Figure S3). The amount of Se(VI)

removed after 22 h increased from only 22% to 89% when the dosage was increased from 1 to 2 g/L, but 100% of the Se(VI) was removed when using dosages of 4 and 5 g/L. However, at short exposure times, the 5 g/L dosage was more effective for removing higher amounts of selenate, with 83% removed after 30 min compared to < 14% for dosages < 4 g/L. When using 5 g/L LDH-500C in the other spiked power plant waters, the removal efficacy increased to 100% for almost of all of the waters (Figure 2b). These results show that LDH-based media is a good candidate to remove Se from power plant waters, even when there are much higher levels of sulfate (hundreds of ppm-level) compared to Se(VI).

3.3. Small-Scale Column Test (1.1 cm Diameter)

Small-scale column tests can be effective tools for assessing important characteristics of sorbent media, such as the empty-bed contact time (EBCT), loading capacity, and breakthrough curve characteristics using less media, water, and evaluation time than a large scale column test [60]. Figure S4 shows a photograph of the column loaded with the LDH media. The breakthrough curve for the column test conducted on the as-obtained CT blowdown water (initial total [Se] = 2.67 ppb and [S] = 187 ppm) and the results are shown in Figure 3 and Table 1, respectively. In Table S2, these results are further compared with those obtained from a small-scale column test performed using the same LDH granular media to remove Se from the makeup water (groundwater) used to supply the cooling tower in our previous study [44]. The adsorption capacity of the LDH in the CT blowdown was determined to be 0.55 μg Se/g LDH, which was lower than what was observed in groundwater (0.65 μg Se/g LDH). Both the [Se] and [S] levels were higher in the CT blowdown compared to the groundwater, but the [S]/[Se] ratio of the CT blowdown was also higher, at 70,000 compared to a ratio of only 21,000 for the groundwater. The exhaustion capacity (Q_e) of the granular LDH in the CT blowdown for S was determined to be 42 mg/g from the breakthrough curve, which was much higher than that for the Se and also the Q_e observed for S in the groundwater test (18 mg/g). The similar breakthrough volumes (V_b in Table 1) for S and Se suggested that the selenate binding sites were saturated by sulfate.

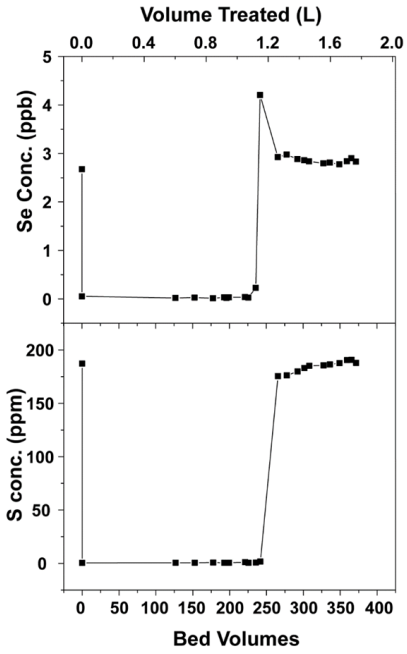

Figure 3. Se and S breakthrough curves of 1.1 cm diameter column test with granular layered double hydroxide (LDH) as bed material to treat cooling tower blowdown water.

Consistent with the jar tests conducted on spiked power plant waters (Figure 2), these results showed that the LDH had better efficacy for selenium removal in waters with lower levels of competing

sulfate anions. However, the Q_e values were only slightly decreased when using the media to treat CT blowdown compared to groundwater (Table S2), despite the much higher [S]/[Se] in the latter case. Based on these promising results, further studies were conducted in the column testbed and pilot unit as described in the next sections.

Table 1. Test results for LDH removal of Se and S from CT blowdown water in small-scale column.

Element	V_b [1]	BV_b [2]	Q_b [3]	V_e [4]	BV_e [5]	Q_e [6]	AER [7]	V_{1g} [8]
Se	1.07	226	0.53 µg/g	1.14	239	0.55 µg/g	4.73	0.21
S	1.14	241	39.79 mg/g	1.26	266	41.87 mg/g	4.26	0.23

[1] Volume (in L) and [2] bed volumes of water treated at breakthrough; [3] Capacity of loading Se or S at breakthrough; [4] Volume (in L) and [5] bed volumes of water treated at bed exhaustion; [6] Exhaustion capacity; [7] Adsorption exhaustion rate; [8] Volume (in L) of water that can be treated with 1 g of sorbent.

3.4. Column Testbed (2"= 5.08 cm Diameter)

A photograph of the testbed used for the scaled-up evaluation of the LDH media is shown in Figure S5. CT blowdown and power plant discharge waters were obtained from Salt River Project for the column tests and detailed information about the composition of these test waters is shown in Table S3. Continuous monitoring of the influent and effluent streams did not show significant changes in the temperature during the ca. 1000 bed volumes of column testing, whereas there were some observed changes in conductivity after startup that stabilized after 100 bed volumes (Figure S6).

As shown by the results in Tables 2 and 3, a higher volume of plant discharge water could be treated compared to the CT blowdown before bed exhaustion. Figure 4 shows the breakthrough curves for Se and S for both types of water. These results can be attributed to the slightly higher sulfate concentration in the CT blowdown, which resulted in a [S]/[Se] ratio of 144,000 compared to 86,000 in the plant discharge, while the initial Se levels in both waters was similar at ~1.2 ppb. In each case, the breakthrough for Se and S occurred at similar bed volumes. An analysis of the ratio of effluent concentration to initial influent concentration (C/C_0) for each species (shown in the insets in Figure 4) revealed that concentration and desorption of the sorbed species could be observed in some cases. For example, this was seen for Se in the CT blowdown, where the concentration in the effluent was almost 2X that of the influent feed. The observation of the leaching spike for Se in the CT blowdown could be explained by the higher concentration of competing sulfate anions contributing to the desorption of the bound Se from the LDH media. It was not clear why the desorption of adsorbed sulfate was observed prominently in the plant discharge column test, and to a lesser extent in the CT blowdown water one.

Table 2. Test results for LDH removal of Se and S from cooling tower (CT) blowdown water in testbed column.

Element	V_b [1]	BV_b [2]	Q_b [3]	V_e [4]	BV_e [5]	Q_e [6]	AER [7]	V_{1g} [8]
Se	149	74	0.16 µg/g	200	100	0.19 µg/g	5.64	0.18
S	159	79	24.75 mg/g	642	320	62.24 mg/g	1.76	0.57

[1] Volume (L) and [2] bed volumes of water treated at breakthrough; [3] Capacity of loading Se or S at breakthrough; [4] Volume (L) and [5] bed volumes of water treated at bed exhaustion; [6] Exhaustion capacity; [7] Adsorption exhaustion rate; [8] Volume (L) of water that can be treated with 1 g of sorbent.

Table 3. Test results for LDH removal of Se and S from plant discharge in testbed column.

Element	V_b [1]	BV_b [2]	Q_b [3]	V_e [4]	BV_e [5]	Q_e [6]	AER [7]	V_{1g} [8]
Se	421	210	0.43 µg/g	869	433	0.65 µg/g	1.45	0.69
S	421	210	36.75 mg/g	747	372	51.01 mg/g	1.69	0.59

[1] Volume (L) and [2] bed volumes of water treated at breakthrough; [3] Capacity of loading Se or S at breakthrough; [4] Volume (L) and [5] bed volumes of water treated at bed exhaustion; [6] Exhaustion capacity; [7] Adsorption exhaustion rate; [8] Volume (L) of water that can be treated with 1 g of sorbent.

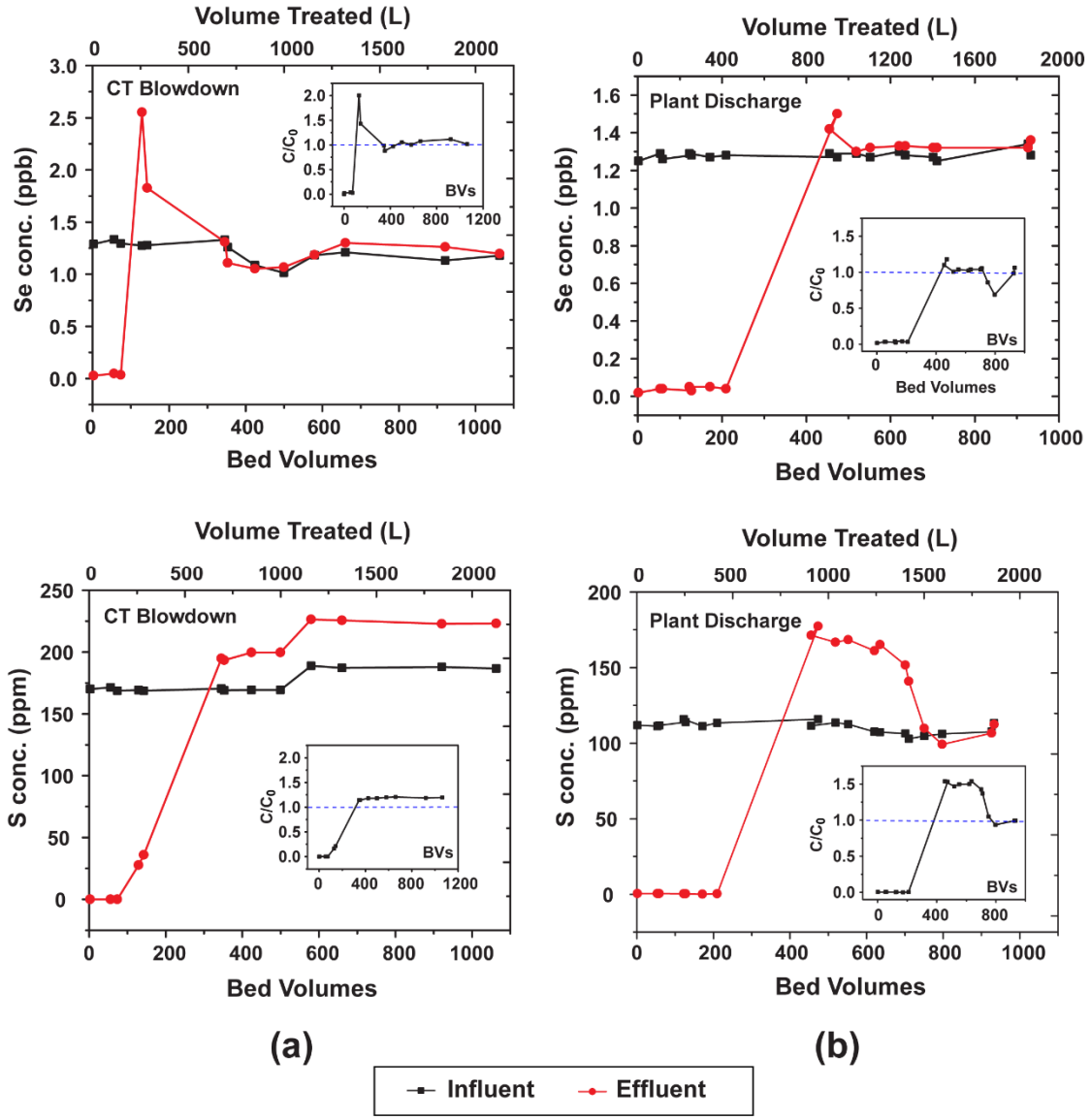

Figure 4. Se and S breakthrough curves from 2″ (5.08 cm) diameter column test (testbed) with granular LDH as bed material to treat (**a**) cooling tower blowdown and (**b**) plant discharge wastewater. Insets show the ratio of effluent to initial influent (C_0) concentration vs. number of bed volumes.

The concentrations of other ions in the waters was also monitored. The influent and effluent levels of select ions are shown in Figure 5 for the CT blowdown and in Figure S7 for the plant discharge. In both waters, the effluent [Al] increased to many ppm levels from the initial level < 4 ppb (Table S3), and gradually decreased as the volume of treated water increased with the level stabilized at ~500 BVs. This implied that Al^{3+} leaching from the LDH occurred. On the other hand, the [Mg] decreased from ~40–50 ppm in the influent to very low levels until breakthrough occurred, indicating removal of Mg^{2+} from the feed solution. Plotting C/C_0 showed that the magnesium concentration was nearly 2X that of the influent, suggesting that Mg^{2+} could be leaching from the LDH, similar to Al^{3+} (Figure S8), although this could also be from release of Mg that had been removed from the influent. The breakthrough volume for Mg in each case was the same as that observed in the S and Se breakthrough curves, which suggests that the processes would be related.

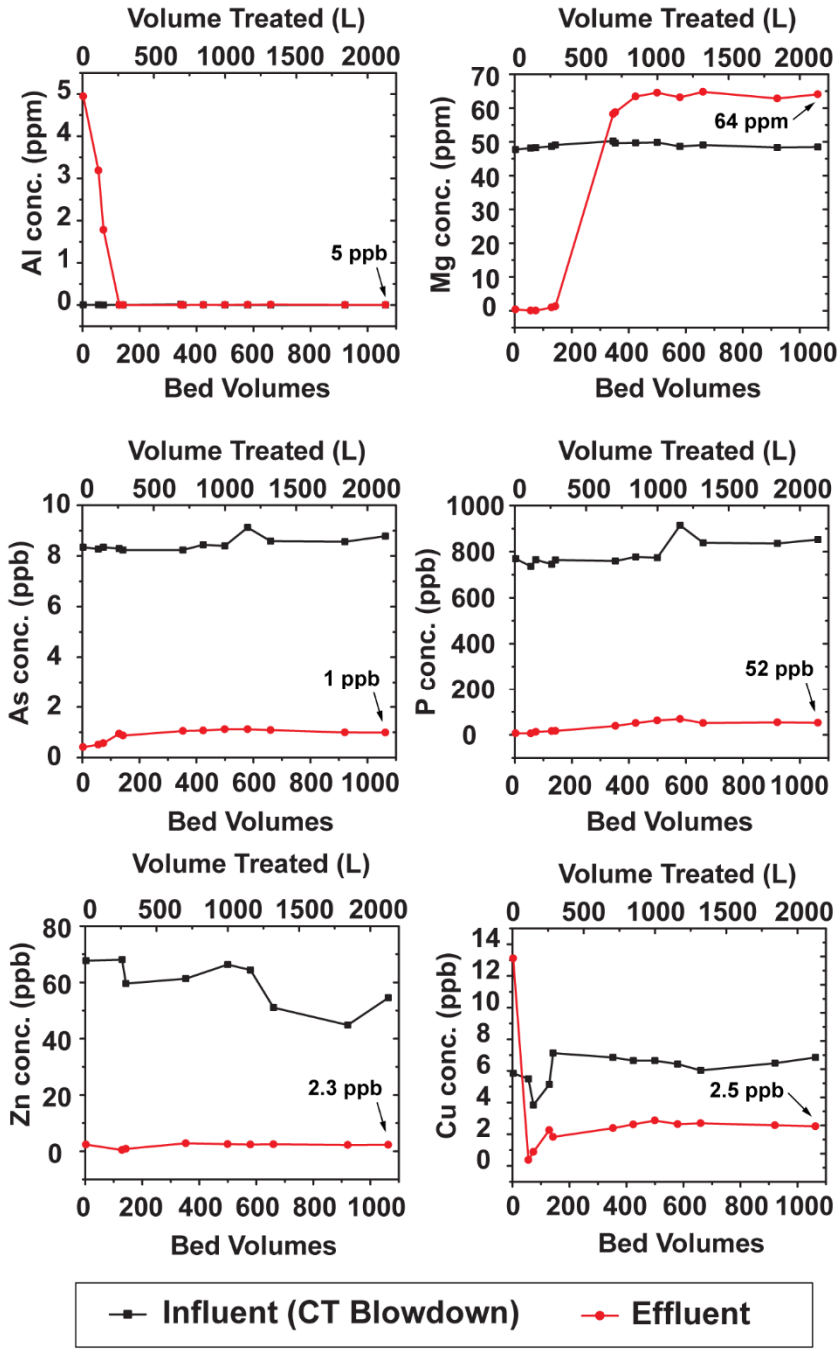

Figure 5. Concentration of select ions in CT blowdown water influent and effluent from testbed.

In the CT blowdown, the As, P, Zn, and Cu levels were significantly reduced and did not indicate that breakthrough occurred within the testing period. Similar observations were made in the plant discharge water. The Cr levels were also monitored in the plant discharge and breakthrough was observed at around 200 BVs, as was observed for Se, S, and Mg (Figure S7). The exhaustion capacity for Cr was determined to be 0.68 µg/g from the breakthrough curve. The UV-vis absorbance analysis of plant discharge water effluent showed a reduction in absorbance at 254 nm, which suggested removal of organic species from the water as well; breakthrough was observed starting at around 200 BVs but approximately 20% capacity still remained after 1000 BVs (Figure S9).

The pH of the influent and effluent waters was also monitored. As shown in Figure 6, there was a large increase of ca. 4 pH units in the effluent upon startup of the column test in both waters. The pH

started to decrease when breakthrough began but was still higher than the influent pH after 1000 BVs. The initial increase in pH was consistent with the basic properties of LDH [61,62] and was confirmed by monitoring the pH increase after immersing the granules into a beaker of DI water (1 g/L dosage); the results showed that the pH of the water increased from 6.43 to above 9.5 within 10 min (Figure S10). The increase in pH also confirmed the ion-exchange mechanism of LDH, whereby the hydroxide and carbonate anions from the LDH interlayer space are replaced with anions from the water [18]. Analysis of the alkalinity (Supplementary Materials, Table S4) showed that both hydroxide and carbonate ions were present as major species in the CT water effluent at 140.5 bed volumes and decreased as the test progressed.

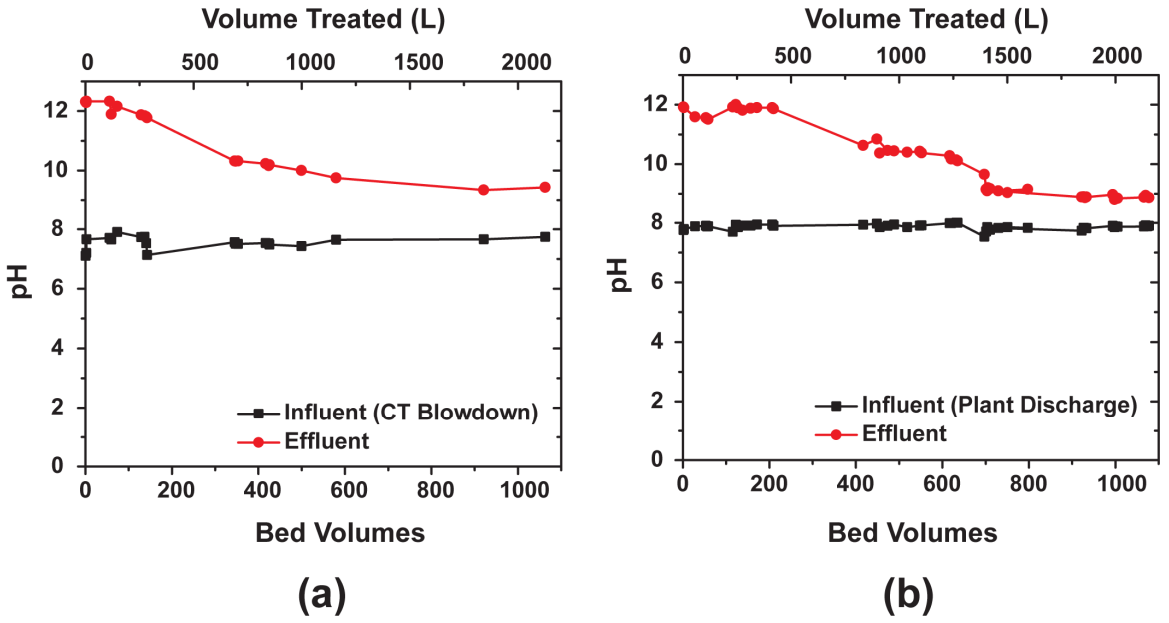

Figure 6. Influent and effluent pH of (**a**) cooling tower blowdown and (**b**) plant discharge wastewater in the testbed column test.

3.5. Pilot-Scale Testing

A pilot unit (Figure S11) was used for online treatment of CT blowdown at Santan Generation Station, which had composition as shown in Table S5. ICP-MS analysis of the initial influent sample showed that the [Se] = 2.74 ppb and [S] = 214 ppm, a [S]/[Se] ratio of approximately 78,000. Several effluent samples (each 250 mL) were pulled over an approximately 1 week period and analyzed with ICP-MS. The flow rates decreased as the test proceeded, and significant biological growth was observed on the top of the media bed (Figure S12). Analysis of the feed solution revealed that the residual chlorine level was only 0.083 mg/L, which is insufficient for prohibiting algae growth [63].

Despite this, as seen by the results in Figure 7, the LDH media was effective for removing Se from the CT blowdown water in actual field conditions. The results also showed that Cr, Mn, Fe, Ni, Cu, Zn, As, and U were also removed. Similar to the laboratory column tests, the Mg levels in the effluent drastically decreased while the Al increased, suggesting removal of Mg^{2+} from the feed solution and leaching of Al^{3+} from the LDH. The pH also increased during the test, from 6.99 in the influent to 11.83 in the first effluent sample pulled (after 1 BV).

The concentration of select anions from the influent and the final effluent sample (77 BVs or 98 gallons of treated water) were analyzed using anion chromatography; the levels of bicarbonate and total dissolved solids (TDS) were also determined (Supplementary Materials). Bromide and fluoride levels were also analyzed but were not detected in the waters. As shown in Table 4, the results showed that orthophosphate, sulfate, and bicarbonate were also successfully removed in the column. Nitrate and chloride were not affected, and TDS levels were only slightly decreased in the effluent.

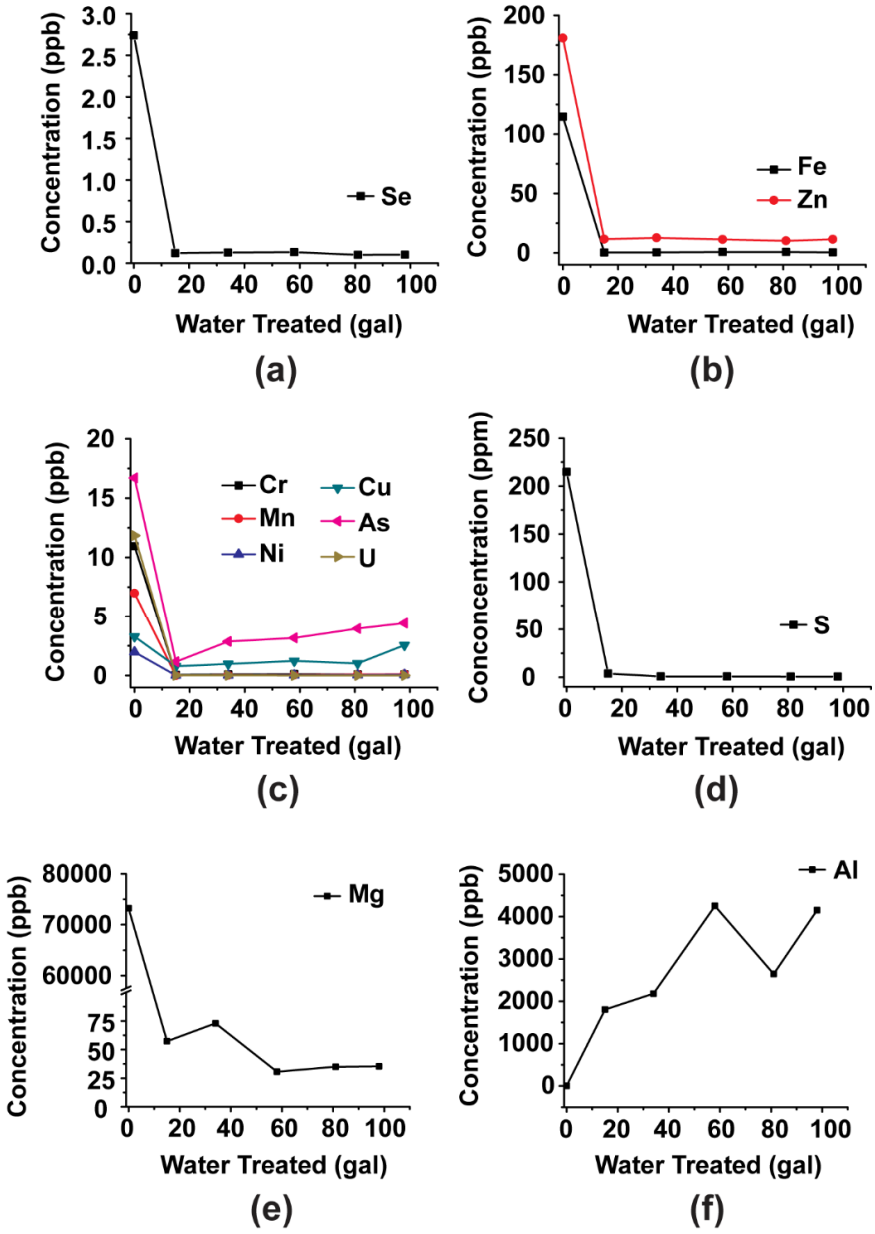

Figure 7. Concentration of select ions in CT blowdown water effluent from pilot test.

Table 4. Comparison of select anion concentrations (in mg/L) in CT blowdown influent and last effluent sample (77 BVs) from on-site pilot test; reporting limits are shown in parentheses.

Water	Nitrate [1]	Orthophosphate [2]	Chloride	Sulfate	Bicarbonate Alkalinity [3]	Total Dissolved Solids
Influent	24 (0.20)	4.2 (0.20)	1300 (40)	870 (40)	74 (6.0)	3700 (100)
Effluent	22 (0.5)	1.42 (0.50)	1300 (40)	ND [4] (2.0)	ND [4] (6.0)	3200 (20)

[1] as N; [2] as P; [3] as $CaCO_3$; [4] Not detected at the reporting limit.

3.6. LDH Post-Mortem Characterization

To understand the breakthrough curve characteristics and the mechanism of removal of contaminants in the aforementioned column tests, a post-mortem analysis was performed on the exhausted LDH media, using X-ray diffraction to assess the changes in LDH crystal structure and FTIR to understand the nature of the species sorbed on the LDH.

3.6.1. X-ray Characterization of LDH after Column Tests

As shown in Figure 8, the XRD pattern of the as-obtained granules showed only two broad peaks associated with the poorly crystalline magnesium/aluminum oxide with cubic periclase structure that is exhibited after LDH is calcined to remove the interlayer anions [47,48]. When immersed into DI water that was sparged with N_2 to remove dissolved CO_2 (from now on, referred to as purged DI water), the brucite-type layers can reform or reconstruct along with the insertion of hydroxide anions and water molecules into the interlayer space [64–67]. The recovery of the layered structure has been referred to as the "memory effect" and is a well-known feature of LDHs.

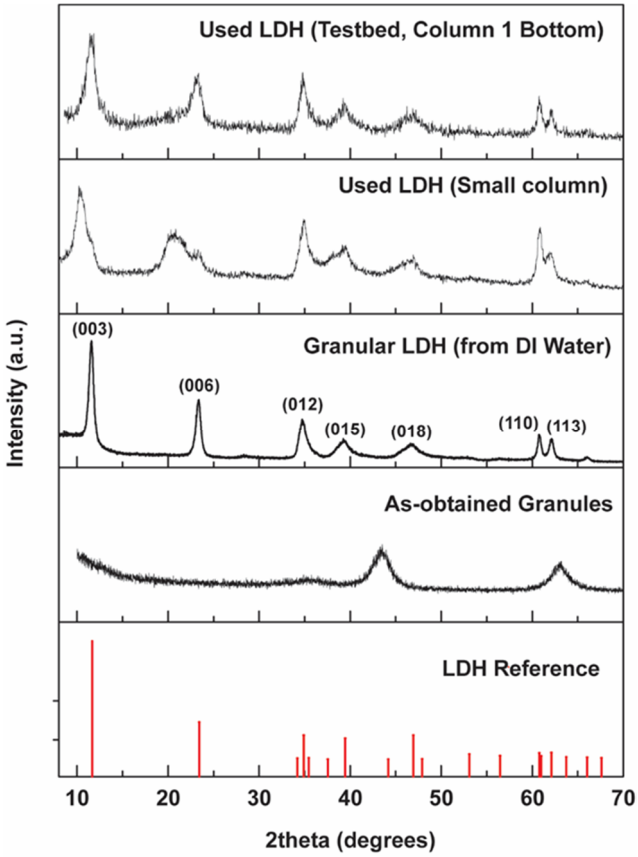

Figure 8. XRD patterns of as-obtained mixed metal oxide granules, granular LDH formed after immersion of as-obtained granules into DI water purged with N_2, and exhausted media from small-scale (1.1 cm) and testbed (2" = 5.08 cm diameter, media taken from bottom of column 1) column tests used for treating CT blowdown. The pattern for $(Mg_{0.667}Al_{0.333})(OH)_2(CO_3)_{0.167}(H_2O)_{0.5}$ from PDF 01-089-0460 is shown as reference.

The (003) reflection for the granules after reconstruction in purged DI water was found at $2\theta = 11.6^\circ$ (d-spacing of 7.63 Å), which is consistent with the presence of interlayer hydroxide and carbonate anions for LDH materials with Mg^{2+}:Al^{3+} of 2:1 (part of the quintinite group of minerals) [21,68,69]. Since the granules were immersed in DI water prior to use in the column tests, the media presumably had a similar layered structure once loaded into the columns. Hence, the removal of anions from the contaminated water would most likely occur through an anion-exchange process, whereby the carbonate and hydroxide anions in the interlayer space would be exchanged with anions from the water. Previous studies have demonstrated that ion-exchange usually occurs with a preference for anions with increasing charge and decreasing size, e.g., $CO_3^{2-} > SO_4^{2-}$, $OH^- > F^- > Cl^- > Br^- > NO_3^- > I^-$ [21,70].

As shown in Figure 8, the exhausted LDH media from the CT blowdown column tests were characterized by broader, less intense reflections overall and a (003) reflection that shifted to lower angles, corresponding to increased d-spacing. XRD analysis of the LDH media from the top and bottom of each of the three testbed columns showed that the patterns looked very similar, suggesting that the sorption was uniformly distributed throughout the entire combined bed (Figure S13a). The average (003) d-spacing for the testbed media samples was 7.69 ± 0.06 Å, consistent with the insertion of larger anions into the interlayer space. For the exhausted LDH granules from the small-scale (1.1 cm) column test, the (003) d-spacing was more notably enlarged to 8.52 Å, which is consistent with LDH containing sulfate in the interlayer space [21,71]. Since the CT blowdown in this particular test had higher concentrations of Se and S compared to the blowdown used for the larger diameter column tests, this feature was attributed to the higher sorption of these species in the LDH interlayers. Some evidence of peak splitting in the (003) and (006) reflections was also observed, which could indicate the presence of multiple anion species of different sizes inside the interlayer region [66,72]. Notably, no other crystalline phases were seen in any of the XRD patterns.

3.6.2. Infrared Analysis of LDH

FTIR spectroscopy was performed to obtain more information regarding changes to the LDH structure after the column tests as well as to identify molecular vibrations of adsorbed species. FTIR spectroscopy of the as-received granules showed characteristics consistent with calcined LDH [38], namely a strong, broad absorption peak centered at around 3440 cm^{-1} (Figure S14) from the stretching bands of hydroxyl groups in the brucite layers [73] and vibrational modes at 1364 cm^{-1} and 853 cm^{-1} which were due to the v_3 and v_2 vibrations, respectively, from interlayer carbonate anions [27,74–76] but no other strong vibrations, indicating the low crystallinity of the mixed metal oxide (Figure 9a, solid trace). The granules were immersed in purged DI water and then dried to use as a reference spectrum for a reconstructed layered structure with predominately interlayer hydroxide, carbonate, and water molecules. The FTIR spectrum of this granular LDH material (Figure 9a, dashed trace) revealed a stronger band associated with interlayer carbonate anions at 1364 cm^{-1}, lattice vibrations of Mg, Al-oxide octahedral sheets at 449 cm^{-1}, Mg/Al-OH translations at 552 cm^{-1}, 669 cm^{-1}, and 775 cm^{-1}, and Al-OH deformation at 933 cm^{-1} [27,28,75]. Because the vibrational frequency of the carbonate fell within the range of 1360–1400 cm^{-1}, this indicated the ions have monodentate coordination and can be readily exchanged with aqueous anions in solution [30].

The FTIR spectrum for the LDH that had been used in the small-scale (1.1 cm) column test for treating CT blowdown (Figure 9b, red trace) had some notable differences compared to the one for the LDH formed after reconstruction of the as-obtained granules in purged DI water. The appearance of the strong band at 1107 cm^{-1} was attributed to interlayer sulfate anions [74,77]. This feature was not as prominent in the spectra obtained from exhausted LDH from the larger column tests (Figure 9c for the testbed column, Figure 9d for the pilot column) likely due to the lower sulfate concentrations in those wastewaters. It should be noted that the FTIR spectra taken of LDH removed from the top and bottom of each of the testbed columns were very similar to each other, confirming (along with the XRD patterns), that the water treatment was uniform over the entire LDH bed (Figure S13b). There were also noticeable changes in the region of the FTIR spectra associated with the LDH lattice vibrations (i.e., for the Mg/Al-O(H) sheets, from 400–900 cm^{-1}), which was also observed in previous studies and reflects the complex surface reactions that occur when selenium and sulfate anions interact with or replace hydroxyl surface groups upon adsorption onto LDH sorbents [28,29].

To identify selenium adsorption on LDH, FTIR spectra were obtained from LDH powder that was exposed to solutions of selenate in DI water (Figure S15). A new band was observed at 859 cm^{-1} and increased in intensity when the concentration of Se(VI) was increased from 50 to 100 ppm, which is consistent with the adsorption of more selenate on the LDH. This band was also consistent with the Se-O vibrational mode reported in the literature [28,29]. However, this mode was not easily discerned in the exhausted LDH media from the column tests, likely due to the low ppb-level of Se in the waters

and the ppm levels of other ions. The weak band observed at 856 cm^{-1} in the used LDH from the pilot column (Figure 9d) could be from adsorbed selenate, but this cannot be conclusively stated as adsorption of arsenic [78,79] and chromium [48,77] oxoanions on LDH materials also give rise to vibrational features in the 830–890 cm^{-1} region (in addition to the aforementioned v_2 mode for carbonate). Hence, making definitive identification of bands in this region is difficult when considering the complex water matrix. On the other hand, the characteristic sharp bands indicating adsorption of nitrate (around 1380–1385 cm^{-1}) [74,77] and phosphate (around 1098 cm^{-1}) [80,81] were not observed.

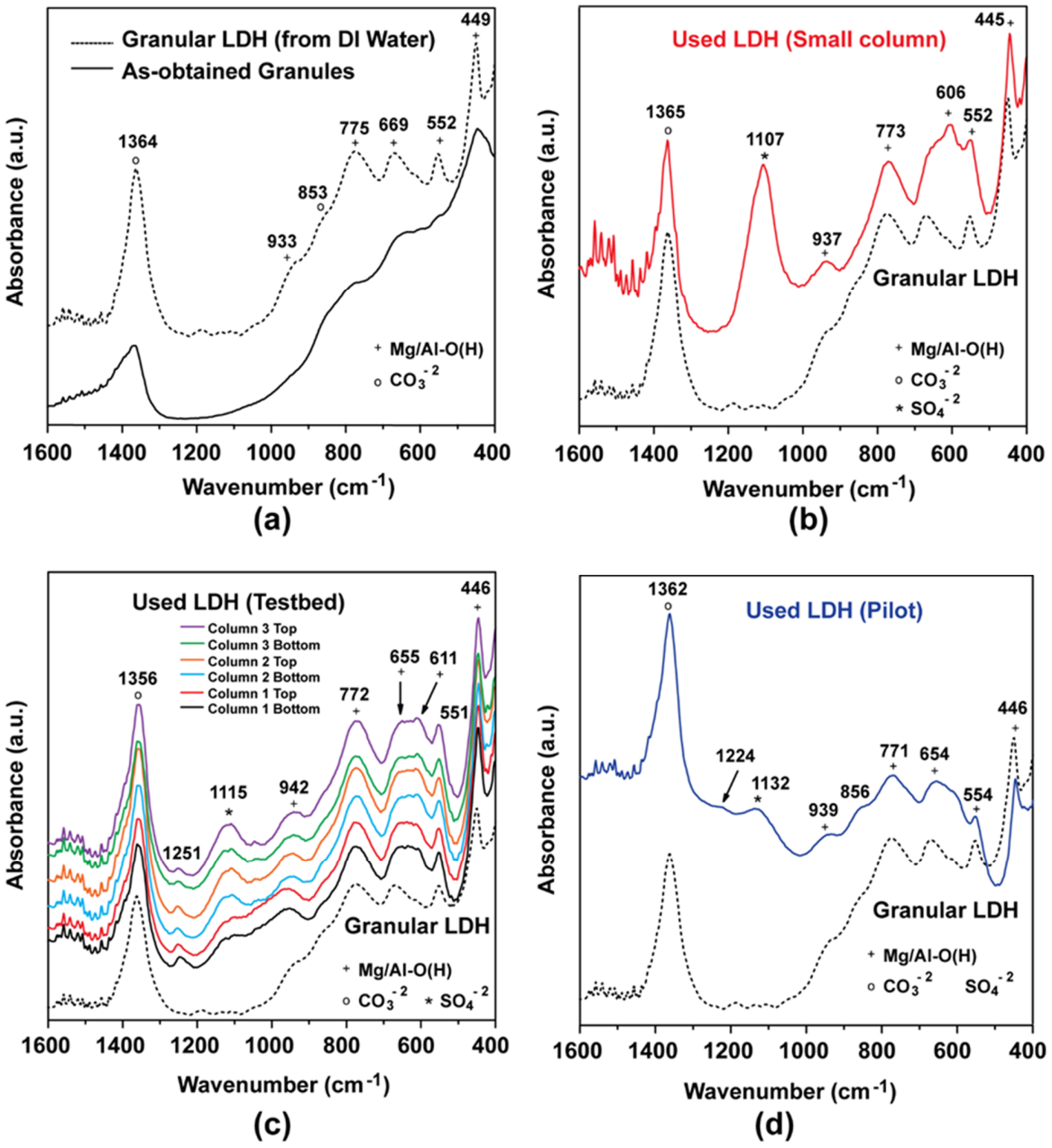

Figure 9. FTIR spectra of (**a**) as-obtained mixed metal oxide granules and used LDH granules from CT blowdown treatment in (**b**) small-scale column test, (**c**) testbed, and (**d**) pilot-scale unit. In each case, the spectrum for the granular LDH (obtained after immersion of the as-obtained granules in DI water purged with N_2) is shown for comparison (dashed line).

3.6.3. LDH Stability Tests

Jar tests were performed to assess the leaching characteristics of the LDH granules used in the column tests, and to better understand the observed Mg and Al levels in the column test effluent. The as-obtained granules were agitated in solutions consisting of DI water with and without 1 ppm Se(VI) and NaOH (to adjust to pH 12) and the water was analyzed for Al, Mg, and Se using ICP-MS after all solids were removed using filtration and centrifugation (Supporting Information).

The results showed that high concentrations of dissolved Mg (almost 2 ppm), and lower amounts of Al (200–300 ppb), were detected in the DI water, while > 4 ppm dissolved Al^{3+} was observed in the pH 12 solutions (Figure 10). However, the equivalent mass loss was very small and amounted to no more than 1 mg (0.5% of the total sorbent mass) that was leached. The slight acidity of the DI water solution could explain the dissolution of Mg^{2+} and Al^{3+} in these solutions, while the precipitation of $Mg(OH)_2$ and solubility of $Al(OH)_3$ at pH > 11 explained the high levels of only Al in the alkaline solutions [82,83]. The presence of Se(VI) in the water and the act of selenate sorption did not appear to affect the Mg and Al leaching, although the %Se removed was slightly lower in the pH 12 solution (Figure S16). These jar test experiments confirm that the increased Al levels observed in the column test effluent were from the LDH media. While Mg may have also been leached from the media (during the rehydration of the granules in DI water prior to loading in the column), the high pH levels of the effluent would have resulted in its precipitation, along with any Mg ions in the feed solutions. However, in both cases the actual mass leached from the LDH was very small, particularly considering the much higher amounts of media used in the column tests compared to the jar tests discussed here.

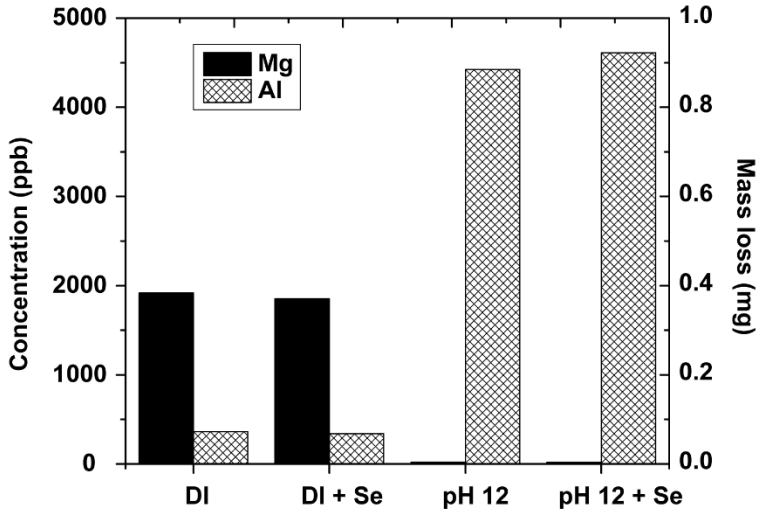

Figure 10. Leaching characteristics of LDH granules. Amount of dissolved Mg and Al after immersing as-obtained granules (0.2 g) in 200 mL of DI water or DI water adjusted to pH 12 with NaOH, with and without 1 ppm Se(VI).

3.7. Regeneration of LDH Media

The memory effect of LDH materials enables the regeneration of the original layered crystal structure after calcined materials are re-exposed to water and other anions [18]. However, previous reports showed reduced sorption capacities for certain anions in the recycled LDH compared to the first use [70,84]. To investigate whether the memory effect phenomenon can be exploited to fully regenerate the exhausted LDH sorbents for selenate adsorption, LDH-500C (5 g/L) was exposed to a DI water solution containing 50 ppm Se(VI); in parallel, another sample of LDH-500C was exposed to 50 ppm sulfate (from Na_2SO_4) with the intent to prepare sorbents saturated with selenate or sulfate. Thermogravimetric analysis (TGA) of these samples showed the removal of interlayer anions between

325–525 °C (Figure S17). Therefore, 550 °C was chosen as the calcination temperature and regeneration was performed by heating the samples for 2 h in a box oven.

The aforementioned LDH-500C samples containing interlayer selenate or sulfate anions were exposed to fresh solutions containing 50 ppm Se(VI). Without using calcination to remove the species adsorbed in the first exposure, less than 40% of the oxoanions could be removed from the waters in the second exposure, as shown in Figure 11. Interestingly, the removal efficacy for Se(VI) after calcination was similar irrespective of which oxoanion the LDH-500C was previously exposed to. The samples were then exposed multiple times to solutions containing 50 ppm Se(VI), with calcination in between each exposure. Both samples showed 100% removal of Se(VI) even after the fifth cycle, indicating that the calcination was effective for regenerating the LDH. The FTIR spectrum of the sorbent after regeneration was very similar to that of the as-prepared LDH-500C (Figure S18), confirming the removal of the adsorbed selenate during the heat treatment. These results showed that after calcination to remove the interlayer anions, the LDH can be reused for subsequent exposures, with the layered structure regenerated each time after adsorbing more selenate anions from water.

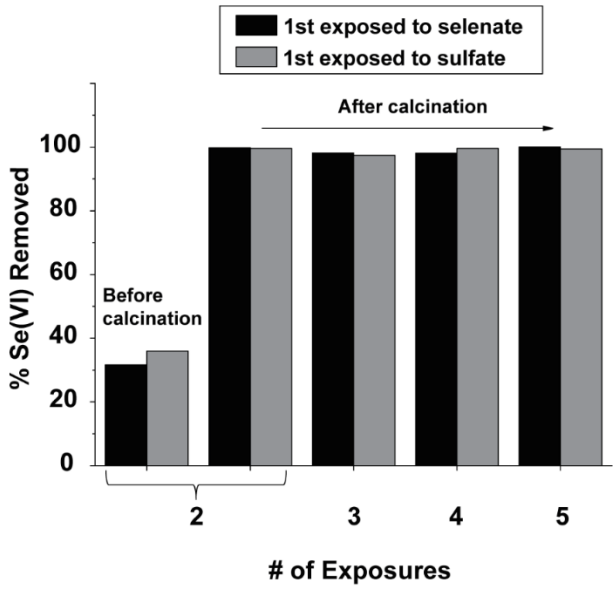

Figure 11. Removal of selenate using LDH-500C that was exposed to 50 ppm selenate or sulfate solution and then regenerated. For each regeneration cycle, the used LDH-500C was calcined at 550 °C for 2 h.

4. Discussion

Our comprehensive investigation of the removal of selenium from power plant wastewaters with varying levels of background ions, coupled with detailed analyses of the water and materials properties, enabled the holistic assessment of LDH sorbents for selenium treatment. The main conclusions and their implications for application of LDH to treat wastewaters will be discussed in the following sections.

4.1. Removal of Selenium and Sulfate Anions

The primary conclusion is that LDH does display efficacy for removing selenium present in power plant wastewater, but the adsorption capacities obtained here are very low (< 1 μg/g exhaustion capacity, ~ 200 BVs treated) due to the following factors: (1) the presence of selenium in low (ppb) levels in the waters investigated here, (2) sulfate anions that are present at much higher concentrations, and (3) the lack of LDH selectivity between these two species. The trend in sorption capacities in the various waters showed more correlation to the [S]/[Se] ratios than to the initial Se concentration, as summarized in Table 5. Chubar et al. reported an LDH sorbent that could treat 4,200 BVs of solution containing 50 ppb of Se(VI) and 0.01 N NaCl as background electrolyte (exhaustion capacity 661 μg/g),

but this subsequently dropped 2.6X to 1,600 BVs (179 µg/g) when a sulfate concentration 74X higher (4.28 ppm) was added [29]. While these sorption capacities are higher than what we found in our studies, the [S]/[Se] ratios were also much higher in our test waters. The lack of LDH selectivity for Se can be addressed by pre-treatment to remove the sulfate, which can lead to higher selenate sorption capacities on LDH as we showed previously [44]. However, the high LDH sorption capacity for sulfate (~50 mg/g observed here) and lack of selectivity with selenate may be useful for applications where simultaneous removal of both species is desired.

Table 5. Test results for LDH removal of Se from column tests. The ground water results are from reference [44].

Wastewater	C_0 (Se) [1] (µg/L)	C_0 (S) [2] (mg/L)	[S]/[Se]	Q_e (Se) [3] (µg/g)	Q_e (S) [4] (mg/g)
Ground water (small-scale column)	1.75	37	21,000	0.65	18
CT blowdown (small-scale column)	2.67	187	70,000	0.55	42
CT blowdown (testbed)	1.22	175	144,000	0.19	62
Plant discharge (testbed)	1.28	110	86,000	0.65	51

[1] Se and [2] S initial concentration, [3] Se and [4] S capacity at breakthrough.

4.2. Effect of pH

Another important feature of the LDH sorbent is its inherent basicity and ability to increase the pH of the treated water > 10 through ion-exchange of hydroxide and carbonate anions with other oxoanions (e.g., selenate, sulfate). The high pH had little negative effect on the efficacy of LDH to remove selenate; moreover, it likely plays a positive role in the removal of other ions from the water (see Section 4.3) through formation of complexes or precipitants. However, the fairly alkaline pH may also lead to increased treatment costs due to the need for acid neutralization afterwards. The apparent exhaustion of the LDH media, as indicated in the breakthrough curve, was dictated by the ion-exchange capacity of the LDH and was correlated with the gradual decrease in pH of the treated water.

4.3. Removal of Other Species from the Water

The pH increase caused by the LDH was most likely responsible for the removal of some of the other ions from water, namely Mg, Cu, Zn, and P. While LDH has been studied as a sorbent for Cu^{2+}, Mg^{2+}, and Zn^{2+} removal, these processes were carried out below pH 6 [85–88]. Hence, the removal of Mg, Cu, and Zn from the wastewaters in our study was likely through precipitation, as $Mg(OH)_2$, $Cu(OH)_2$, and $Zn(OH)_2$ will form above pH 9.5, 7.5, and pH 8.7, respectively [89,90]. The absence of new reflections in the post-mortem XRD patterns (Figure 8) indicated that precipitated compounds (e.g., of Mg, Cu, and Zn hydroxides) were amorphous or in quantities insufficient for detection. It is also possible that the dissolved Mg^{2+} (from the influent) and Al species (leached from the LDH) reacted to form more LDH via co-precipitation in this alkaline environment [91].

Although LDHs have attracted much attention as sorbents for phosphate, there are different removal mechanisms depending on the pH. Many studies have shown the highest P removal at low pH (< 4) where the LDH is partially dissolved; in these cases, the Mg^{2+} and Al^{3+} in solution along with hydroxides can act as coagulants to remove the phosphate [92,93]. Interlayer ion-exchange and surface adsorption is the predominant mechanism at intermediate pH, with phosphate removal usually decreasing > pH 8 due to repulsion by the negative surface charge of the LDH [94,95]. In our case, the high effluent pH and absence of breakthrough for P as was seen for Se and S suggested a different removal mechanism. This was also corroborated by the absence of the characteristic P-O asymmetric stretching at around 1098 cm^{-1} that is an indicator of phosphate adsorption on LDH [80,81] in the

post-mortem FTIR data (Figure 9). It should be noted that the use of chemical precipitation (i.e., addition of calcium salts to an alkalinized solution of phosphate) is a developed technique for P recovery from wastewater, with a precipitation efficiency of 82.7% at pH 11 reported using a Ca/P ratio of 1.5 [96]. In our case, the P removal efficiency was more than 90% with the Ca/P molar ratio in the influent water greatly exceeding 100:1, making this a feasible explanation. The low crystallinity of precipitated calcium phosphates at high pH [97] may explain the absence of reflections from these phases in the XRD patterns as well. Therefore, P removal most likely occurred due to precipitation of other compounds due to the high pH and presence of other complexing ions (e.g., Ca, Al).

Similarly, LDHs can remove arsenic oxoanions via ion-exchange and adsorption with high capacities when the pH is lower than the sorbent's point of zero charge [98], with reduced effectiveness above pH 8 [38,99]. This, along with the fact that phosphate is a known competing anion for arsenate [38] and is present at much higher concentrations in the wastewaters studied here, makes the removal of arsenic oxoanions via ion-exchange seem unlikely. The removal of arsenic through aluminum- or iron-, or calcium-arsenate precipitates could be possible based on the pH of the effluent and previous studies [100,101]. While chromium removal on LDHs was also reduced in high pH solutions [77], the similar breakthrough characteristics for Cr (Figure S7) as for Se and sulfate (Figure 4) indicated it may be removed through a similar ion-exchange mechanism rather than precipitation.

4.4. Stability of LDH

The leaching characteristics of the LDH are largely dependent on the pH of the water. When the as-obtained granules are exposed to slightly acidic DI water for rehydration, Mg and Al ions can dissolve into solution. The dissolution of LDH materials in acidic conditions is well known (total dissolution of LDH is possible < pH 4 [81,82,102]) and has been exploited as a means to deliver pharmaceuticals [103,104]. However, stability studies show that Mg and Al leaching from LDH is minimal at high pH due to the precipitation of $Mg(OH)_2$ and $Al(OH)_3$ [82,83]. In our case, the initial pH increase of the effluent to > 12 at low bed volumes from the ion-exchange process (Figure 6) could lead to dissolution of $Al(OH)_3$ [82,83], resulting in increased Al in the effluent. As the pH decreases, the dissolved Al^{3+} ions could complex with phosphate or arsenic anions, and eventually re-precipitate as $Al(OH)_3$ at pH < 11 [83,105]. The mass loss from leaching was small with respect to the total mass of the sorbent (< 0.5 wt% leached). Even with this observed leaching, the regeneration tests showed that calcination of the LDH media after use was an effective way to reconstruct the materials, with no change in the selenate removal ability observed after numerous regeneration cycles.

5. Conclusions

In this work, a comprehensive investigation of LDH as a sorbent material for removing selenium from real power plant wastewaters was performed.

- LDH granulated media were successfully evaluated under dynamic sorption conditions in laboratory columns and in the field for the removal of selenium from power plant wastewater.
- Continuous monitoring of influent and effluent pH showed the treated water increased to above pH 12 after startup, but gradually decreased after breakthrough of the bed.
- The LDH displayed good adsorption ability for Se(VI) in DI water solutions (66 mg/g equilibrium sorption capacity for calcined powdered media) but this was decreased in the real wastewaters < 1 μg/g due to the presence of competing anion species.
- Simultaneous removal of selenium, sulfate (~50 mg/g) and chromium (< 1 μg/g) was observed, likely occurring through anion-exchange with interlayer hydroxide and carbonate species in the LDH.
- Other species (Mg, Cu, Zn, P, As, Mn, Fe, Ni, U) were also removed from the wastewater, but likely through precipitation.

- Despite some Al^{3+} and Mg^{2+} leaching (< 0.5% of the original mass), the LDH materials retained their crystallinity after use. Calcination was demonstrated to be effective for regenerating the spent materials multiple times without losing selenate adsorption capacity.

Supplementary Materials: The following are available online at http://www.mdpi.com/2305-7084/3/1/20/s1, Details of the experimental methods, materials and procedures; Scheme S1: Structure of as-obtained granules and powder and processing conditions, Figure S1: XRD and SEM characterization of LDH-500C, Figure S2: FTIR spectra of LDH-500C, Figure S3: Effect of LDH dosage on Se(VI) removal, Figure S4: Photograph of small-scale column setup, Figure S5: Photograph of testbed, Figure S6: Conductivity and temperature of influent and effluent from the testbed studies, Figure S7: Concentration of select ions in plant discharge wastewater influent and effluent from testbed studies, Figure S8: Ratio of effluent to influent (C/C_0) levels for Al and Mg in testbed, Figure S9: UV-vis absorbance results from testbed, Figure S10: Jar test study monitoring pH change, Figure S11: Photograph of pilot skid, Figure S12: Photograph of biological growth in pilot column, Figure S13: XRD and FTIR of exhausted testbed media, Figure S14: Wide-range FTIR comparison, Figure S15: FTIR characterization of selenate adsorption onto LDH, Figure S16. Effect of pH on Se(VI) removal, Figure S17: TGA data of different LDHs, Figure S18: FTIR spectra of different LDHs, Table S1: pH and Se levels in power plant wastewater jar tests, Table S2: Comparison of small-scale column test results, Table S3: Water composition of wastewaters treated in the testbed evaluation of LDH, Table S4: Alkalinity (in mg/L) for effluent samples from CT blowdown column test as determined using titration, Table S5: Water composition of test waters for pilot test.

Author Contributions: Conceptualization, C.K.C., L.M.F., S.S.; investigation, M.L., T.C., H.J., A.N.K., A.D.; formal analysis, M.L., C.K.C., S.S.; writing—original draft, C.K.C. and M.L.; writing—review and editing, C.K.C., M.L., S.S., T.C., H.J., A.N.K., A.D., L.M.F.; visualization, C.K.C. and M.L.; supervision, C.K.C., L.M.F., S.S.; project administration, C.K.C.; funding acquisition, C.K.C. and L.M.F.

Funding: This research was funded through the Arizona State University/Salt River Project Joint Research Program, under the projects "Pilot Test on Selenium Removal from SRP Waters using Solid Phase Extraction Materials" and "Column Test Studies on Selenium Removal from SRP Waters using Solid Phase Extraction Materials." Partial support from the National Science Foundation Nanosystems Engineering Research Center for Nanotechnology Enabled Water Treatment (EEC-1449500) is also acknowledged.

Acknowledgments: We would like to thank D. Pelley, F. Fuller, B. Schuster, N. Smith, and L. Bonilla from Salt River Project for their support of this research, for providing water samples, for assistance with the pilot test field study, and for many helpful discussions. We are also grateful to N. Gudovic from Canyon State Filtration for assistance with the pilot test skid design and implementation. We also acknowledge the use of facilities within the Goldwater Environmental Laboratory, Keck Foundation Laboratory for Environmental Biogeochemistry, Goldwater Materials Science Facility, and Nanosystems Engineering Research Center for Nanotechnology-Enabled Water Treatment.

Conflicts of Interest: The authors declare no conflict of interest. The funders had no role in the design of the study; in the collection, analyses, or interpretation of data; in the writing of the manuscript, or in the decision to publish the results.

References

1. Roberts, C. Effluent Limitations Guidelines and Standards for the Steam Electric Power Generating Point Source Category, 40 CFR Part 423. *Fed. Regist.* **2015**, *80*, 67838–67903. Available online: https://www.govinfo.gov/content/pkg/FR-2015-11-03/pdf/2015-25663.pdf (accessed on 3 November 2015).
2. Gingerich, D.B.; Grol, E.; Mauter, M.S. Fundamental Challenges and Opportunities in Flue Gas Desulfurization Wastewater Treatment at Coal Fired Power Plants. *Environ. Sci. Water Res. Technol.* **2018**, *4*, 909–925. [CrossRef]
3. Lemly, A.D. Aquatic Selenium Pollution is a Global Environmental Safety Issue. *Ecotoxicol. Environ. Saf.* **2004**, *59*, 44–56. [CrossRef]
4. Title 18. Environmental Quality. Chapter 11. Department of Environmental Quality-Water Quality Standards. 2016. Available online: https://www.epa.gov/sites/production/files/2014-12/documents/az-chapter11-provisions.pdf (accessed on 15 December 2018).
5. Ohlendorf, H.M. The Birds of Kesterson Reservoir: A Historical Perspective. *Aquat. Toxicol.* **2002**, *57*, 1–10. [CrossRef]
6. Wu, L. Review of 15 Years of Research on Ecotoxicology and Remediation of Land Contaminated by Agricultural Drainage Sediment Rich in Selenium. *Ecotoxicity Environ. Saf.* **2004**, *57*, 257–269. [CrossRef]
7. Tan, L.C.; Nancharaiah, Y.V.; van Hullebusch, E.D.; Lens, P.N.L. Selenium: Environmental Significance, Pollution, and Biological Treatment Technologies. *Biotechnol. Adv.* **2016**, *34*, 886–907. [CrossRef] [PubMed]

8. *Review of Available Technologies for the Removal of Selenium from Water*; Final Report prepared for North American Metals Council. CH2MHill: Englewood, CO, USA, 2010. Available online: http://www.namc.org/docs/00062756.PDF (accessed on 1 January 2013).
9. Santos, S.; Ungureanu, G.; Boaventura, R.; Botelho, C. Selenium Contaminated Waters: An Overview of Analytical Methods, Treatment Options and Recent Advances in Sorption Methods. *Sci. Total Environ.* **2015**, *521–522*, 246–260. [CrossRef]
10. Holmes, A.B.; Gu, F.X. Emerging Nanomaterials for the Application of Selenium Removal for Wastewater Treatment. *Environ. Sci. Nano* **2014**, *3*, 982–996. [CrossRef]
11. Sonstegard, J.; Pickett, T.; Harwood, J.; Johnson, D. Full Scale Operation of GE ABMet®Biological Technology for the Removal of Selenium from FGD Wastewaters. In *69th Annual International Water Conference*; Curran Associates, Inc.: San Antonio, TX, USA, 2008.
12. *Biological Treatment of Flue Gas Desulfurization Wastewater at a Power Plant Burning Powder River Basin Coal: Pilot Demonstration with the ABMet Technology*; Final Report 3002006089; Electric Power Research Institute: Palo Alto, CA, USA, 2017. Available online: https://www.epri.com/#/pages/product/3002006089/?lang=en-US (accessed on 15 December 2018).
13. Peak, D.; Sparks, D.L. Mechanisms of Selenate Adsorption on Iron Oxides and Hydroxides. *Environ. Sci. Technol.* **2002**, *36*, 1460–1466. [CrossRef]
14. Elzinga, E.J.; Tang, Y.; McDonald, J.; Desisto, S.; Reeder, R.J. Macroscopic and Spectroscopic Characterization of Selenate, Selenite, and Chromate Adsorption at the Solid-Water Interface of Gamma-Al_2O_3. *J. Colloid Interface Sci.* **2009**, *340*, 153–159. [CrossRef]
15. Johnston, C.P.; Chrysochoou, M. Mechanisms of Chromate, Selenate, and Sulfate Adsorption on Al-Substituted Ferrihydrite: Implications for Ferrihydrite Surface Structure and Reactivity. *Environ. Sci. Technol.* **2016**, *50*. [CrossRef] [PubMed]
16. Zhang, N.; Dianchen Gang, D.; Mcdonald, L.; Lin, L.-S. Background Electrolytes and pH Effects on Selenate Adsorption Using Iron-Impregnated Granular Activated Carbon and Surface Binding Mechanisms. *Chemosphere* **2018**, *195*, 166–174. [CrossRef] [PubMed]
17. Cavani, F.; Trifirb, F.; Vaccari, A. Hydrotalcite-Type Anionic Clays: Preparation, Properties and Applications. *Catal. Today* **1991**, *11*, 172–301. [CrossRef]
18. Goh, K.H.; Lim, T.T.; Dong, Z. Application of Layered Double Hydroxides for Removal of Oxyanions: A Review. *Water Res.* **2008**, *42*, 1343–1368. [CrossRef] [PubMed]
19. Liang, X.; Zang, Y.; Xu, Y.; Tan, X.; Hou, W.; Wang, L.; Sun, Y. Sorption of Metal Cations on Layered Double Hydroxides. *Colloids Surfaces A Physicochem. Eng. Asp.* **2013**, *433*, 122–131. [CrossRef]
20. Bo, A.; Sarina, S.; Liu, H.; Zheng, Z.; Xiao, Q.; Gu, Y.; Ayoko, G.A.; Zhu, H. Efficient Removal of Cationic and Anionic Radioactive Pollutants from Water Using Hydrotalcite-Based Getters. *ACS Appl. Mater. Interfaces* **2016**, *8*, 16503–16510. [CrossRef] [PubMed]
21. Miyata, S. Anion-Exchange Properties of Hydrotalcite-Like Compounds. *Clays Clay Miner.* **1983**, *31*, 305–311. [CrossRef]
22. Mills, S.J.; Christy, A.G.; Génin, J.-M.R.; Kameda, T.; Colombo, F. Nomenclature of the hydrotalcite supergroup: natural layered double hydroxides. *Mineral. Mag.* **2012**, *76*, 1289–1336. [CrossRef]
23. You, Y.; Vance, G.F.; Zhao, H. Selenium Adsorption on Mg-Al and Zn-Al Layered Double Hydroxides. *Appl. Clay Sci.* **2001**, *20*, 13–25. [CrossRef]
24. Tsuji, M. SeO_3^{2-}-Selective Properties of Inorganic Materials Synthesized by the Soft Chemical Process. *Solid State Ionics* **2002**, *151*, 385–392. [CrossRef]
25. Constantino, L.V.; Nunes Quirino, J.; Monteiro, A.M.; Abrao, T.; Parreira, P.S.; Urbano, A.; Santos, M.J. Sorption-Desorption of Selenite and Selenate on Mg-Al Layered Double Hydroxide in Competition with Nitrate, Sulfate and Phosphate. *Chemosphere* **2017**, *181*, 627–634. [CrossRef] [PubMed]
26. Chubar, N. New Inorganic (An)ion Exchangers Based on Mg-Al Hydrous Oxides: (Alkoxide-Free) Sol-Gel Synthesis and Characterisation. *J. Colloid Interface Sci.* **2011**, *357*, 198–209. [CrossRef] [PubMed]

27. Chubar, N.; Gerda, V.; Megantari, O.; Mičušík, M.; Omastova, M.; Heister, K.; Man, P.; Fraissard, J. Applications versus Properties of Mg-Al Layered Double Hydroxides Provided by Their Syntheses Methods: Alkoxide and Alkoxide-Free Sol-Gel Syntheses and Hydrothermal Precipitation. *Chem. Eng. J.* **2013**, *234*, 284–299. [CrossRef]
28. Chubar, N. EXAFS and FTIR Studies of Selenite and Selenate Sorption by Alkoxide-Free Sol-Gel Generated Mg-Al-CO_3 Layered Double Hydroxide with Very Labile Interlayer Anions. *J. Mater. Chem. A* **2014**, *2*, 15995–16007. [CrossRef]
29. Chubar, N.; Szlachta, M. Static and Dynamic Adsorptive Removal of Selenite and Selenate by Alkoxide-Free Sol-Gel-Generated Mg-Al-CO_3 Layered Double Hydroxide: Effect of Competing Ions. *Chem. Eng. J.* **2015**, *279*, 885–896. [CrossRef]
30. Chubar, N.; Gilmour, R.; Gerda, V.; Mičušík, M.; Omastova, M.; Heister, K.; Man, P.; Fraissard, J.; Zaitsev, V. Layered Double Hydroxides as the Next Generation Inorganic Anion Exchangers: Synthetic Methods versus Applicability. *Adv. Colloid Interface Sci.* **2017**, *245*, 62–80. [CrossRef]
31. Chubar, N. The Influence of Sulfate on Selenate Sorption on Mg-Al-CO_3 Layered Double Hydroxides Prepared by Fine Inorganic Sol-Gel Synthesis Studied by X-ray Photoelectron Spectroscopy. *Appl. Surf. Sci.* **2018**, *459*, 281–291. [CrossRef]
32. Koilraj, P.; Kamura, Y.; Sasaki, K. Carbon-Dot-Decorated Layered Double Hydroxide Nanocomposites as a Multifunctional Environmental Material for Co-immobilization of SeO_4^{2-} and Sr^{2+} from Aqueous Solutions. *ACS Sustain. Chem. Eng.* **2017**, *5*, 9053–9064. [CrossRef]
33. Koilraj, P.; Kamura, Y.; Sasaki, K. Cosorption Characteristics of SeO_4^{2-} and Sr^{2+} Radioactive Surrogates Using 2D/2D Graphene Oxide-Layered Double Hydroxide Nanocomposites. *ACS Sustain. Chem. Eng.* **2018**, *6*, 13854–13866. [CrossRef]
34. Asiabi, H.; Yamini, Y.; Shamsayei, M. Highly Selective and Efficient Removal of Arsenic(V), Chromium(VI) and Selenium(VI) Oxyanions by Layered Double Hydroxide Intercalated with Zwitterionic Glycine. *J. Hazard. Mater.* **2017**, *339*, 239–247. [CrossRef]
35. Das, J.; Das, D.; Dash, G.P.; Parida, K.M. Studies on Mg/Fe Hydrotalcite-Like-Compound (HTlc) I. Removal of Inorganic Selenite (SeO_3^{2-}) from Aqueous Medium. *J. Colloid Interface Sci.* **2002**, *251*, 26–32. [CrossRef]
36. Chen, M.-L.; An, M.-I. Selenium Adsorption and Speciation with Mg-FeCO_3 Layered Double Hydroxides Loaded Cellulose Fibre. *Talanta* **2012**, *95*, 31–35. [CrossRef]
37. Das, N.N.; Konar, J.; Mohanta, M.K.; Srivastava, S.C. Adsorption of Cr(VI) and Se(IV) from their Aqueous Solutions onto Zr^{4+}-Substituted ZnAl/MgAl-Layered Double Hydroxides: Effect of Zr^{4+} Substitution in the Layer. *J. Colloid Interface Sci.* **2004**, *270*, 1–8. [CrossRef]
38. Yang, L.; Shahrivari, Z.; Liu, P.K.T.; Sahimi, M.; Tsotsis, T.T. Removal of Trace Levels of Arsenic and Selenium from Aqueous Solutions by Calcined and Uncalcined Layered Double Hydroxides (LDH). *Ind. Eng. Chem. Res.* **2005**, *44*, 6804–6815. [CrossRef]
39. Das, J.; Sairam Patra, B.; Baliarsingh, N.; Parida, K. Calcined Mg-Fe-CO_3 LDH as an Adsorbent for the Removal of Selenite. *J. Colloid Interface Sci.* **2007**, *316*, 216–223. [CrossRef]
40. Liu, R.; Frost, R.L.; Martens, W.N. Absorption of the Selenite Anion from Aqueous Solutions by Thermally Activated Layered Double Hydroxide. *Water Res.* **2009**, *43*, 1323–1329. [CrossRef]
41. Paikaray, S.; Hendry, M.J.; Essilfie-Dughan, J. Controls on Arsenate, Molybdate, and Selenate Uptake by Hydrotalcite-Like Layered Double Hydroxides. *Chem. Geol.* **2013**, *345*, 130–138. [CrossRef]
42. Ma, L.; Islam, S.M.; Xiao, C.; Zhao, J.; Liu, H.; Yuan, M.; Sun, G.; Li, H.; Ma, S.; Kanatzidis, M.G. Rapid Simultaneous Removal of Toxic Anions $[HSeO_3]^-$, $[SeO_3]^{2-}$, and $[SeO_4]^{2-}$, and Metals Hg^{2+}, Cu^{2+}, and Cd^{2+} by MoS_4^{2-} Intercalated Layered Double Hydroxide. *J. Am. Chem. Soc.* **2017**, *139*, 12745–12757. [CrossRef]
43. Tian, N.; Zhou, Z.; Tian, X.; Yang, C.; Li, Y. Superior Capability of $MgAl_2O_4$ for Selenite Removal from Contaminated Groundwater During its Reconstruction of Layered Double Hydroxides. *Sep. Purif. Technol.* **2017**, *176*, 66–72. [CrossRef]
44. Li, M.; Farmen, L.M.; Chan, C.K. Selenium Removal from Sulfate-Containing Groundwater Using Granular Layered Double Hydroxide Materials. *Ind. Eng. Chem. Res.* **2017**, *56*, 2458–2465. [CrossRef]
45. Feeley, T.J.; Skone, T.J.; Stiegel, G.J.; McNemar, A.; Nemeth, M.; Schimmoller, B.; Murphy, J.T.; Manfredo, L. Water: A Critical Resource in the Thermoelectric Power Industry. *Energy* **2008**, *33*, 1–11. [CrossRef]
46. Li, M.; Dopilka, A.; Kraetz, A.N.; Jing, H.; Chan, C.K. Layered Double Hydroxide/Chitosan Nanocomposite Beads as Sorbents for Selenium Oxoanions. *Ind. Eng. Chem. Res.* **2018**, *57*, 4978–4987. [CrossRef]

47. Miyata, S. Physico-Chemical Properties of Synthetic Hydrotalcites in Relation to Composition. *Clays Clay Miner.* **1980**, *28*, 50–56. [CrossRef]
48. Martinez-Gallegos, S.; Pfeiffer, H.; Lima, E.; Espinosa, M.; Bosch, P.; Bulbulian, S. Cr(VI) Immobilization in Mixed (Mg, Al) Oxides. *Microporous Mesoporous Mater.* **2006**, *94*, 234–242. [CrossRef]
49. Yang, W.; Kim, Y.; Liu, P.K.T.; Sahimi, M.; Tsotsis, T.T. A Study by In Situ Techniques of the Thermal Evolution of the Structure of a Mg-Al-CO_3 Layered Double Hydroxide. *Chem. Eng. Sci.* **2002**, *57*, 2945–2953. [CrossRef]
50. Yamani, J.S.; Lounsbury, A.W.; Zimmerman, J.B. Adsorption of Selenite and Selenate by Nanocrystalline Aluminum Oxide, Neat and Impregnated in Chitosan Beads. *Water Res.* **2014**, *50*, 373–381. [CrossRef]
51. Fu, Y.; Wang, J.; Liu, Q.; Zeng, H. Water-Dispersible Magnetic Nanoparticle–Graphene Oxide Composites for Selenium Removal. *Carbon* **2014**, *77*, 710–721. [CrossRef]
52. Das, S.; Hendry, J.; Essilfie-Dughan, J. Adsorption of Selenate onto Ferrihydrite, Goethite, and Lepidocrocite under Neutral pH Conditions. *Appl. Geochem.* **2013**, *28*, 185–193. [CrossRef]
53. Martínez, M.; Giménez, J.; de Pablo, J.; Rovira, M.; Duro, L. Sorption of Selenium(IV) and Selenium(VI) onto Magnetite. *Appl. Surf. Sci.* **2006**, *252*, 3767–3773. [CrossRef]
54. Gonzalez, C.M.; Hernandez, J.; Parsons, J.G.; Gardea-Torresdey, J.L. Adsorption of Selenite and Selenate by a High- and Low- Pressure Aged Manganese Oxide Nanomaterial. *Instrum. Sci. Technol.* **2011**, *39*, 1–19. [CrossRef]
55. Gonzalez, C.M.; Hernandez, J.; Parsons, J.G.; Gardea-Torresdey, J.L. A Study of the Removal of Selenite and Selenate from Aqueous Solutions using a Magnetic Iron/Manganese Oxide Nanomaterial and ICP-MS. *Microchem. J.* **2010**, *96*, 324–329. [CrossRef]
56. Bleiman, N.; Mishael, Y.G. Selenium Removal from Drinking Water by Adsorption to Chitosan—Clay Composites and Oxides: Batch and Columns Tests. *J. Hazard. Mater.* **2010**, *183*, 590–595. [CrossRef]
57. Chan, Y.T.; Kuan, W.H.; Chen, T.Y.; Wang, M.K. Adsorption Mechanism of Selenate and Selenite on the Binary Oxide Systems. *Water Res.* **2009**, *43*, 4412–4420. [CrossRef]
58. Salt River Project (Tempe, AZ, USA). Personal communication, 2014.
59. Jegadeesan, G.; Mondal, K.; Lalvani, S.B. Selenate Removal from Sulfate Containing Aqueous Solutions. *Environ. Technol.* **2005**, *26*, 1181–1187. [CrossRef]
60. Westerhoff, P.; Highfield, D.; Badruzzaman, M.; Yoon, Y. Rapid Small-Scale Column Tests for Arsenate Removal in Iron Oxide Packed Bed Columns. *J. Environ. Eng.* **2005**, *131*, 262–271. [CrossRef]
61. Constantino, V.R.L.; Pinnavaia, T.J. Basic Properties of $Mg^{2+}_{1-x}Al^{3+}_{x}$ Layered Double Hydroxides Intercalated by Carbonate, Hydroxide, Chloride, and Sulfate Anions. *Inorg. Chem.* **1995**, *34*, 883–892. [CrossRef]
62. Di Cosimo, J.I.; Díez, V.K.; Xu, M.; Iglesia, E.; Apesteguía, C.R. Structure and Surface and Catalytic Properties of Mg-Al Basic Oxides. *J. Catal.* **1998**, *178*, 499–510. [CrossRef]
63. Brungs, W.A. Effects of residual chlorine on aquatic life. *Water Pollut. Control Fed.* **1973**, *45*, 2180–2193.
64. Rey, F.; Fornes, V.; Rojo, J.M. Thermal Decomposition of Hydrotalcites An Infrared and Nuclear Magnetic Resonance Spectroscopic Study. *J. Chem. Soc. Faraday Trans.* **1992**, *88*, 2233–2238. [CrossRef]
65. Millange, F.; Walton, R.I.; O'Hare, D. Time-Resolved In Situ X-ray Diffraction Study of the Liquid-Phase Reconstruction of Mg-Al-Carbonate Hydrotalcite-Like Compounds. *J. Mater. Chem.* **2000**, *10*, 1713–1720. [CrossRef]
66. Erickson, K.L.; Bostrom, T.E.; Frost, R.L. A Study of Structural Memory Effects in Synthetic Hydrotalcites Using Environmental SEM. *Mater. Lett.* **2005**, *59*, 226–229. [CrossRef]
67. Theiss, F.L.; Palmer, S.J.; Ayoko, G.A.; Frost, R.L. Sulfate Intercalated Layered Double Hydroxides Prepared by the Reformation Effect. *J. Therm. Anal. Calorim.* **2012**, *107*, 1123–1128. [CrossRef]
68. Zhitova, E.S.; Krivovichev, S.V.; Pekov, I.V.; Yakovenchuk, V.N.; Pakhomovsky, Y.A. Correlation Between the *d*-value and the M^{2+}:M^{3+} Cation Ratio in Mg-Al-CO_3 Layered Double Hydroxides. *Appl. Clay Sci.* **2016**, *130*, 2–11. [CrossRef]
69. Bellotto, M.; Rebours, B.; Clause, O.; Lynch, J.; Bazin, D.; Elkaïm, E. A Reexamination of Hydrotalcite Crystal Chemistry. *J. Phys. Chem.* **1996**, *100*, 8527–8534. [CrossRef]
70. Parker, L.M.; Milestone, N.B.; Newman, R.H. The Use of Hydrotalcite as an Anion Absorbent. *Ind. Eng. Chem. Res.* **1995**, *34*, 1196–1202. [CrossRef]
71. Bookin, A.S.; Cherkashin, V.I.; Drits, V.A. Polytype Diversity of the Hydrotalcite-like Minerals II. Determination of the Polytypes of Experimentally Studied Varieties. *Clays Clay Miner.* **1993**, *41*, 558–564. [CrossRef]

72. Tsujimura, A.; Uchida, M.; Okuwaki, A. Synthesis and Sulfate Ion-Exchange Properties of a Hydrotalcite-Like Compound Intercalated by Chloride Ions. *J. Hazard. Mater.* **2007**, *143*, 582–586. [CrossRef]
73. Kustrowski, P.; Sułkowska, D.; Chmielarz, L.; Rafalska-Łasocha, A.; Dudek, B.; Dziembaj, R. Influence of Thermal Treatment Conditions on the Activity of Hydrotalcite-Derived Mg-Al Oxides in the Aldol Condensation of Acetone. *Microporous Mesporous Mater.* **2004**, *78*, 11–22. [CrossRef]
74. Hernandez-Moreno, M.J.; Ulibarri, M.A.; Rendon, J.L.; Serna, C.J. IR Characteristics of Hydrotalcite-like Compounds. *Phys. Chem. Miner.* **1985**, *12*, 34–38. [CrossRef]
75. El Gaini, L.; Lakraimi, M.; Sebbar, E.; Meghea, A.; Bakasse, M. Removal of Indigo Carmine Dye from Water to Mg-Al-CO_3-Calcined Layered Double Hydroxides. *J. Hazard. Mater.* **2009**, *161*, 627–632. [CrossRef]
76. Palmer, S.J.; Frost, R.L.; Nguyen, T. Hydrotalcites and Their Role in Coordination of Anions in Bayer Liquors: Anion Binding in Layered Double Hydroxides. *Coord. Chem. Rev.* **2009**, *253*, 250–267. [CrossRef]
77. Khitous, M.; Salem, Z.; Halliche, D. Effect of Interlayer Anions on Chromium Removal Using Mg-Al Layered Double Hydroxides: Kinetic, Equilibrium and Thermodynamic Studies. *Chin. J. Chem. Eng.* **2016**, *24*, 433–445. [CrossRef]
78. Prasanna, S.V.; Kamath, P.V. Synthesis and Characterization of Arsenate-Intercalated Layered Double Hydroxides (LDHs): Prospects for Arsenic Mineralization. *J. Colloid Interface Sci.* **2009**, *331*, 439–445. [CrossRef] [PubMed]
79. Huang, P.-P.; Cao, C.-Y.; Wei, F.; Sun, Y.-B.; Song, W.-G. MgAl Layered Double Hydroxides with Chloride and Carbonate Ions as Interlayer Anions for Removal of Arsenic and Fluoride Ions in Water. *RSC Adv.* **2015**, *5*, 10412–10417. [CrossRef]
80. Shimamura, A.; Jones, M.I.; Kanezaki, E.; Metson, J.B. Complete Desorption of Interlayer Hydrogen Phosphate in Mg/Al-Layered Double Hydroxides by Means of Anion Exchange with 1-Octanesulfonate. *J. Mater. Sci.* **2012**, *47*, 1142–1147. [CrossRef]
81. Luengo, C.V.; Volpe, M.A.; Avena, M.J. High Sorption of Phosphate on Mg-Al Layered Double Hydroxides: Kinetics and Equilibrium. *J. Environ. Chem. Eng.* **2017**, *5*, 4656–4662. [CrossRef]
82. Jobbágy, M.; Regazzoni, A.E. Dissolution of Nano-Size Mg-Al-Cl Hydrotalcite in Aqueous Media. *Appl. Clay Sci.* **2011**, *51*, 366–369. [CrossRef]
83. Xu, S.; Liao, M.-C.; Zeng, H.-Y.; Liu, X.-J.; Du, J.-Z.; Ding, P.-X.; Zhang, W. Surface Modification and Dissolution Behavior of Mg-Al Hydrotalcite Particles. *J. Taiwan Inst. Chem. Eng.* **2015**, *56*, 174–180. [CrossRef]
84. Elhalil, A.; Qourzal, S.; Mahjoubi, F.Z.; Elmoubarki, R.; Farnane, M.; Tounsadi, H.; Sadiq, M.; Abdennouri, M.; Barka, N. Defluoridation of Groundwater by Calcined Mg/Al Layered Double Hydroxide. *Emerg. Contam.* **2016**, *2*, 42–48. [CrossRef]
85. Komarneni, S.; Kozai, N.; Roy, R. Novel Function for Anionic Clays: Selective Transition Metal Cation Uptake by Diadochy. *J. Mater. Chem.* **1998**, *8*, 1329–1331. [CrossRef]
86. Richardson, M.C.; Braterman, P.S. Cation Exchange by Anion-Exchanging Clays: The Effects of Particle Aging. *J. Mater. Chem.* **2009**, *19*, 7965–7975. [CrossRef]
87. Yang, F.; Sun, S.; Chen, X.; Chang, Y.; Zha, F.; Lei, Z. Mg-Al Layered Double Hydroxides Modified Clay Adsorbents for Efficient Removal of Pb^{2+}, Cu^{2+} and Ni^{2+} from Water. *Appl. Clay Sci.* **2016**, *123*, 134–140. [CrossRef]
88. Yue, X.; Liu, W.; Chen, Z.; Lin, Z. Simultaneous Removal of Cu(II) and Cr(VI) by Mg-Al-Cl Layered Double Hydroxide and Mechanism Insight. *J. Environ. Sci.* **2017**, *53*, 16–26. [CrossRef] [PubMed]
89. Albrecht, T.W.J.; Addai-Mensah, J.; Fornasiero, D. Effect of pH, Concentration and Temperature on Copper and Zinc Hydroxide Formation/Precipitation in Solution. In *CHEMECA 2011 - "Engineering a Better World"*; Institution of Engineers Australia: Barton, Australia, 2011; pp. 1–10.
90. Um, N.; Hirato, T. Precipitation Behavior of $Ca(OH)_2$, $Mg(OH)_2$, and $Mn(OH)_2$ from $CaCl_2$, $MgCl_2$, and $MnCl_2$ in NaOH-H_2O Solutions and Study of Lithium Recovery from Seawater via Two-Stage Precipitation Process. *Hydrometallurgy* **2014**, *146*, 142–148. [CrossRef]
91. Boclair, J.W.; Braterman, P.S. Layered Double Hydroxide Stability. 1. Relative Stabilities of Layered Double Hydroxides and Their Simple Counterparts. *Chem. Mater.* **1999**, *11*, 298–302. [CrossRef] [PubMed]
92. Seida, Y.; Nakano, Y. Removal of Phosphate by Layered Double Hydroxides Containing Iron. *Water Res.* **2002**, *36*, 1306–1312. [CrossRef]

93. Novillo, C.; Guaya, D.; Allen-Perkins Avendaño, A.; Armijos, C.; Cortina, J.L.; Cota, I. Evaluation of Phosphate Removal Capacity of Mg/Al Layered Double Hydroxides from Aqueous Solutions. *Fuel* **2014**, *138*, 72–79. [CrossRef]
94. Ookubo, A.; Ooi, K.; Hayashi, H. Preparation and Phosphate Ion-Exchange Properties of a Hydrotalcite-like Compound. *Langmuir* **1993**, *9*, 1418–1422. [CrossRef]
95. Iftekhar, S.; Küçük, M.E.; Srivastava, V.; Repo, E.; Sillanpaa, M. Application of Zinc-Aluminium Layered Double Hydroxides for Adsorptive Removal of Phosphate and Sulfate: Equilibrium, Kinetic and Thermodynamic. *Chemosphere* **2018**, *209*, 470–479. [CrossRef]
96. Tran, A.T.K.; Zhang, Y.; De Corte, D.; Hannes, J.-B.; Ye, W.; Mondal, P.; Jullok, N.; Meesschaert, B.; Pinoy, L.; Van Der Bruggen, B. P-Recovery as Calcium Phosphate from Wastewater Using an Integrated Selectrodialysis/Crystallization Process. *J. Clean. Prod.* **2014**, *77*, 140–151. [CrossRef]
97. Mekmene, O.; Quillard, S.; Rouillon, T.; Bouler, J.-M.; Piot, M.; Gaucheron, F. Effects of pH and Ca/P Molar Ratio on the Quantity and Crystalline Structure of Calcium Phosphates Obtained from Aqueous Solutions. *Dairy Sci. Technol.* **2009**, *89*, 301–316. [CrossRef]
98. Wang, J.; Zhang, T.; Li, M.; Yang, Y.; Lu, P.; Ning, P.; Wang, Q. Arsenic Removal from Water/Wastewater Using Layered Double Hydroxide Derived Adsorbents, A Critical Review. *RSC Adv.* **2018**, *8*, 22694–22709. [CrossRef]
99. Violante, A.; Pucci, M.; Cozzolino, V.; Zhu, J.; Pigna, M. Sorption/Desorption of Arsenate on/from Mg-Al Layered Double Hydroxides: Influence of Phosphate. *J. Colloid Interface Sci.* **2009**, *333*, 63–70. [CrossRef] [PubMed]
100. Hyun Moon, D.; Dermatas, D.; Menounou, N. Arsenic Immobilization by Calcium-Arsenic Precipitates in Lime Treated Soils. *Sci. Total Environ.* **2004**, *330*, 171–185. [CrossRef] [PubMed]
101. Violante, A.; Pigna, M.; Del Gaudio, S.; Cozzolino, V.; Banerjee, D. Coprecipitation of Arsenate with Metal Oxides. 3. Nature, Mineralogy, and Reactivity of Iron(III)-Aluminum Precipitates. *Environ. Sci. Technol.* **2009**, *43*, 1515–1521. [CrossRef] [PubMed]
102. Parello, M.L.; Rojas, R.; Giacomelli, C.E. Dissolution Kinetics and Mechanism of Mg-Al Layered Double Hydroxides: A Simple Approach to Describe Drug Release in Acid Media. *J. Colloid Interface Sci.* **2010**, *351*, 134–139. [CrossRef] [PubMed]
103. Rives, V.; Del Arco, M.; Martín, C. Layered Double Hydroxides as Drug Carriers and for Controlled Release of Non-Steroidal Antiinflammatory Drugs (NSAIDs): A Review. *J. Control. Release* **2013**, *169*, 28–39. [CrossRef] [PubMed]
104. Rives, V.; Del Arco, M.; Martín, C. Intercalation of Drugs in Layered Double Hydroxides and Their Controlled Release: A Review. *Appl. Clay Sci.* **2014**, *88–89*, 239–269. [CrossRef]
105. Zhi, P.X.; Guo, Q.L. Hydrothermal Synthesis of Layered Double Hydroxides (LDHs) from Mixed MgO and Al_2O_3: LDH Formation Mechanism. *Chem. Mater.* **2005**, *17*, 1055–1062. [CrossRef]